Chapter 1
Fundamentals in Adsorption at the Solid-Gas Interface. Concepts and Thermodynamics

Vera Bolis

Abstract Some fundamental concepts about the features of a solid material surface and the adsorption at the gas-solid interface are illustrated. The basic tools dealing with the thermodynamics aspects of adsorption processes are also discussed. The stepwise adsorption microcalorimetry technique, which is a tool of greatest quantitative merit in surface chemistry studies, is described in detail through a selection of gas-solid interface systems, taken from different materials science fields. Criteria for discriminating physical and chemical adsorption are given, based on the nature of the forces involved in the process and the heat of adsorption values. The molecular interpretation of the volumetric-calorimetric data, favored by the joint use of adsorption microcalorimetry, spectroscopic and/or *ab initio* modeling techniques, is also stressed by illustrating a number of examples dealing with either physical or associative/dissociative chemical adsorption.

1.1 Introduction

Phenomena taking place at the solid-fluid interface are governed by specific and/or aspecific interactions between the atoms at the solid surface and the molecules approaching the surface from the gas (or the liquid) phase. In particular, heterogeneous catalysis is based on a sequence of steps which involve adsorption of reactants at the surface of the solid material, surface reactions and desorption of final products [1, 2]. On the other hand, the adsorption of (bio)molecules at the solid surface of biomaterials in contact with physiological fluids is recognized to be the initial step of a chain of molecular events leading to the favorable integration of the implanted material [3, 4]. The adsorption features of (probe) molecules on solid surfaces have been

V. Bolis (✉)
Dipartimento di Chimica and NIS Centre of Excellence, Università di Torino,
Via Pietro Giuria 7, 10125 Torino, Italy
e-mail: vera.bolis@gmail.com

A. Auroux (ed.), *Calorimetry and Thermal Methods in Catalysis*,
Springer Series in Materials Science 154, DOI: 10.1007/978-3-642-11954-5_1,

studied over the years by a variety of different techniques, which allowed to describe the nature of the fluid-solid interactions and give insight into the properties of the solid surface [1, 2, 5, 6]. On one hand, spectroscopic techniques (in particular, IR and Raman, UV-vis, NMR, XPS, EXAFS-XANES) are suitable methods to describe the microscopic features of the solid, i.e., the nature and structure of both surface terminations and adsorbed species formed upon contact with molecules [7–9]. On the other hand, adsorption microcalorimetry represents a tool of greatest quantitative merit in that the heat evolved when a fluid contacts the solid surface is related to the nature and energy of the adsorbed species/surface atoms interactions [10–16]. Further, the knowledge of the energetics of chemical and physical events responsible for the process as well as the assessment of the associated thermodynamic parameters contributes to a thorough understanding of phenomena taking place at both catalytic and biological interfaces [13–17]. Coupling the molar volumetric-calorimetric data with the molecular information on the nature of the interaction arising from both spectroscopic methods and *ab initio* computational results, has been proved very fruitful in characterizing in the surface acidity of materials [16, 18–29].

1.2 The Solid Surface

When a molecule (or an atom) from the gas-phase approaches a solid, it is more or less strongly attracted by the atoms exposed at the surface, according to the nature of both the molecule and the solid material.

A crystalline solid is described through the periodic infinite repetition of an elemental pattern (unit cell) [1]. A real solid is however necessarily finite: the periodic repetition of the unit cell terminates generating a surface, the structure of which depends on the cleavage of the crystal, the chemical (either ionic or covalent) nature of the solid and the origin of the surface (either chemical or mechanical). The surface atoms arrangement depends on the plane preferentially exposed during the formation of the surface, according to the preparation conditions of the real material (either in the single crystal form or as nanosized powder) [30]. If no major reconstruction processes are required in order to minimize the surface atoms energy, and if no structural/compositional defects are present, an ideal perfect homogeneous surface is obtained which can be properly represented by cutting a slab of the solid structure. Such an ideal perfect homogeneous surface is very rarely encountered, unless especially prepared for surface science studies. Real solid surfaces (mostly in the case of finely divided, nanometric sized solids) are made up of a combination of flat regions (terraces), structural defects (steps, kinks, corners, edges), point defects (vacancies of ions/atoms in the solid), as schematically illustrated in Fig. 1.1 Compositional defects may contribute to the "imperfections" of the solid surface. They include a variety of oxidation states of the atoms constituting the solid and/or a variety of heteroatoms present either as impurities, or especially introduced in order to modify the physico-chemical properties of the surface. This means that in a real solid

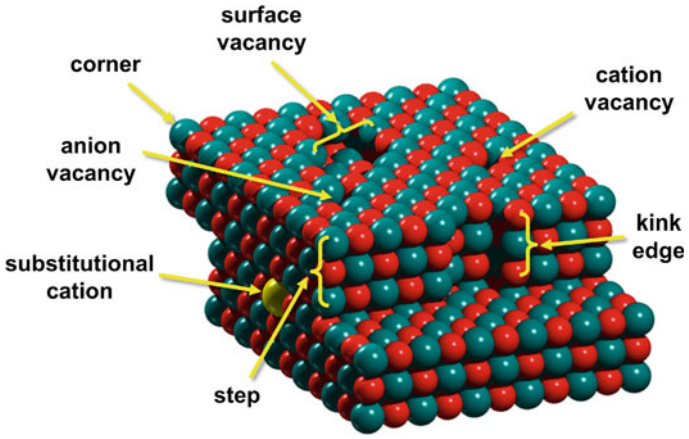

Fig. 1.1 Cartoon of a piece of realistic MgO nanocrystal, which exhibits both structural (steps, kinks edges and corners) and point (anionic and cationic vacancies) defects along the flat regions (terraces). The presence of a compositional defect (substitutional cation) is also outlined. By courtesy of Prof. Piero Ugliengo, University of Torino

a heterogeneous distribution of surface sites potentially active in catalytic reactions and/or in interface processes is generally expected.

Another type of heterogeneous solid surface is represented by an active material dispersed *ad hoc* over the surface of another solid (the support) [31].

In recent years, with the advent of high resolution electron microscopes it has become possible to image atomic details in nanocrystals [9]. Some of the above mentioned structural defects can be imaged by the high resolution transmission electron microscopy (HR-TEM), as illustrated in Fig. 1.2 for monoclinic ZrO_2 nanocrystals, which terminate with structural defects as steps, kinks edges and corners [19].

Owing to their intrinsic coordinative and/or valence unsaturation, species making up such defects act as surface highly reactive sites capable of taking up molecules from the environment.

1.2.1 Porous Materials

Finely divided solids possess not only a geometrical surface, as defined by the different planes exposed by the solid, but also an internal surface due to the primary particles aggregation, which generates pores of different size according to both the nature of the solid and origin of the surface. Pores are classified on the basis of their width w, which represents either the diameter of a cylindrical pore, or the distance between the sides of a slit-shaped pore [32]. The smallest pores, characterized by a width $w < 20$ Å (2 nm) are defined *micropores*; the intermediate pores, characterized by a width comprised in the 20 Å $\leq w \leq$ 500 Å (2 and 50 nm) range are classified as

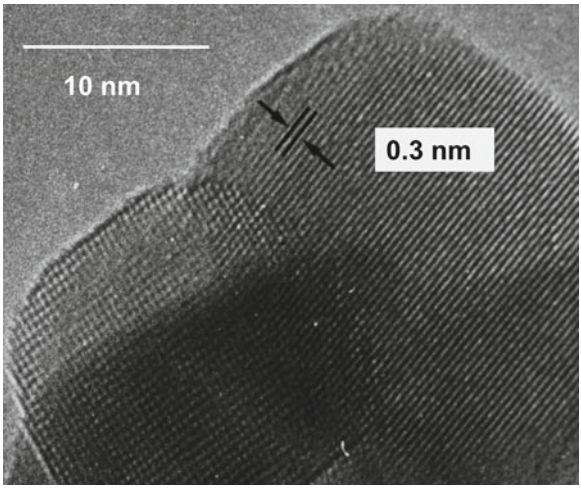

Fig. 1.2 High resolution transmission electron microscopy (HR-TEM) of monoclinic ZrO2 nanocrystals. Adapted from Ref. [19], Fig.2a

mesopores, whereas the largest pores, characterized by a width $w > 500$ Å (50 nm) as *macropores* [31, 32].

Some materials, like charcoal and silico-alumina, have irregular pores with widely variable diameters in a normal shape. Conversely, other materials such as zeolites and clay minerals are entirely micro- or meso-porous, respectively. In these cases, the porosity does not arise from the primary particles aggregation but is an intrinsic structural feature of the solid material [31, 33, 34].

Zeolites are either natural or synthetic crystalline alumino-silicates, the structure of which is based upon a three dimensional polymeric framework, with nanosized cages and channels [1, 2, 33–35]. The basic building block of such materials, of general formula $M^{n+}_{x/n}\left[(AlO_2)_x\,(SiO_2)_y\right]^{x-}\cdot zH_2O$, is the $[TO_4]$ unit with $T = Si, Al$. This unit is a tetrahedron centered on one T atom bound to four O atoms located at the corners; each O atom is in turn shared between two T atoms. These tetrahedral units join each another through T−O−T linkages in a variety of open-structure frameworks characterized by (interconnected) channels and voids which are occupied by cations and water molecules. The presence of charge-balancing (extra-framework) cations is required in order to compensate the negative charge of the tetrahedral $[AlO_4]^-$ units in which Al is in isomorphous substitution of Si atoms. The density of charge-balancing cations depends upon the $\frac{Si}{Al}$ ratio, which span in the 1 to ∞ range (for $\frac{Si}{Al} \rightarrow \infty$ the so-called all-silica zeolites are obtained) [36–38]. The nature and distribution of extra-framework cations, which are intrinsically mobile and can be exchanged by other cations (including the acidic proton) give specific chemical properties to the material. On the other hand, the presence of nanosized cages and channels within the crystalline structure of zeolites gives to these materials unique molecular sieve

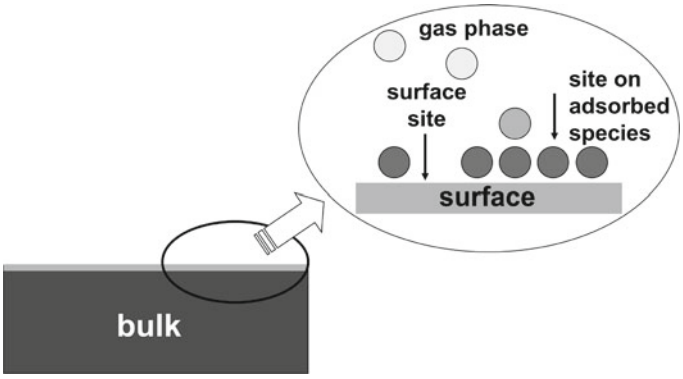

Fig. 1.3 Schematic picture of adsorption process at the surface of a solid material

and shape selectivity properties, of greatest interest in catalysis and in gas separation processes [1, 2, 33, 34, 38, 39].

In all cases, porous materials exhibit high surface areas, which maximize the extension of the interface region.

1.3 Adsorption Processes

The surface atoms of a solid, which are coordinatively unsaturated with respect to the bulk atoms, become saturated thanks to the interaction with molecules of the environment. Adsorption is the process whereby molecules from the gas (or liquid) phase are taken up by a solid surface; it is distinguished from absorption which refers to molecules entering into the lattice (bulk) of the solid material. The adsorptive is the material in the gas phase capable of being adsorbed, whereas the adsorbate is the material actually adsorbed by the solid. The solid, which exposes the surface sites responsible for the process is called the adsorbent. In Fig. 1.3 the adsorption process at the surface of a solid material is schematically illustrated.

Adsorption is governed by either physical or chemical forces. In the former case the adsorption is named physical adsorption (*physisorption*) whereas in the latter case chemical adsorption (*chemisorption*). Details on the nature of these forces will be dealt in Sect. 1.6, through the description of a selection of examples.

When a solid is exposed in a closed space to a gas at pressure p, the weight of the solid typically increases and the pressure of the gas decreases: the gas is adsorbed by the solid. After a time, the pressure p does not change any more and correspondingly the weight ceases to increase any further: a dynamic equilibrium is reached. The amount of gas adsorbed is experimentally determined: (i) by gravimetry (the increase in weight of the solid is monitored by a spring balance); (ii) by volumetry (the fall in the gas pressure is monitored by manometers/transducer gauges); (iii) by

monitoring the change of any other physical parameter related to the adsorption of matter, such as the evolved heat (if the heat of adsorption is known and constant) or the integrated IR absorbance (if the specific molar absorbance of adsorbed species is known) [20, 40–42].

1.3.1 Adsorption Isotherms

Adsorption is described through isotherms, i.e., through the functions connecting the amount of adsorbate taken up by the adsorbent (or the change of any other physical parameter related to the adsorption of matter) with the adsorptive equilibrium pressure p, the temperature T and all other parameters being constant. Below the critical temperature the pressure is properly normalized to the saturation vapor pressure p°, and the adsorbed amounts are so referred to the dimensionless relative pressure, $\frac{p}{p^{\circ}}$.

Adsorption isotherms are currently classified in five classes (I - V) according to the Brunauer, Deming, Deming, Teller (BDDT) original classification, [43] which is often referred to as the Brunauer, Emmet, and Teller (BET), [44] or simply to as the Brunauer [45] classification. An extra type of isotherm (the stepped Type VI isotherm, which is relatively rare) is also reported. Type IV and V isotherms typically exhibit a hysteresis loop, which is characteristic of porous systems, involving capillary condensation [32].

The fractional coverage θ of the adsorbate, at a given equilibrium pressure p, is defined as the ratio of N_S surface sites occupied by the adsorbate over the total available adsorption sites N, i.e. the total number of substrate surface sites which are active towards the given adsorptive. The first layer of adsorbed phase is due to either *chemisorption* or *physisorption*, or both, according to the nature of the forces governing the adsorbate/adsorbent interactions (*vide infra* Sect. 1.6). Conversely, the second layer is originated by physical forces, similar to the forces that lead to the non-ideal behavior of gases and eventually to the condensation to the liquid. Subsequent layers are expected to approach a liquid-like phase.

When the number of N_S occupied sites matches the number of total available sites N, the adsorbate monolayer is complete ($\theta = 1$). In Fig. 1.4 the formation of subsequent layers of adsorbate at the surface of a solid sample is schematically illustrated.

The amount of gas taken up by a solid surface depends upon the solid and the gas nature, the pressure p of the gas and the temperature T. The uptake being proportional to the mass m and the surface area A of the sample, adsorbed amounts (often expressed as mass or volume *STP* of the gas) are properly normalized either to the unit mass or to the unit surface area. Here, in view of describing the process at molecular details, the adsorbed amounts n_{ads} are properly expressed as adsorbate moles (or molecules) per either unit mass or unit surface area of the adsorbent.

As an example, in Fig. 1.5 the equilibrium data for CO adsorbed at $T = 303\,\mathrm{K}$ on Na− and K−MFI zeolites, are reported as volumetric (Fig. 1.5a) and calorimetric (Fig. 1.5b) isotherms. In volumetric isotherms the adsorbed amounts (n_{ads}), in calori-

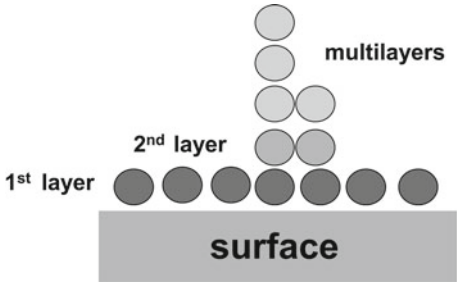

Fig. 1.4 Schematic illustration of the first and second layer of adsorption; the multi-layers adsorption approaches a liquid-like phase

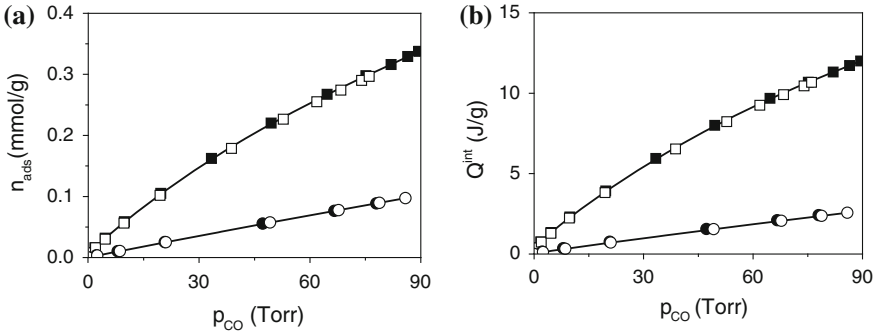

Fig. 1.5 Adsorption of CO at $T = 303$ K on Na–MFI (*square*) and K–MFI (*circle*) zeolites outgassed at $T = 673$ K. **a** Volumetric isotherms (adsorbed amounts vs. equilibrium pressure). **b** Calorimetric isotherms (evolved heats vs. equilibrium pressure). *Solid symbols* first run, *open symbols* second run of adsorption. Experimental points interpolated by the Langmuir equation (*vide infra*)

metric isotherms the integral heat (Q^{int}) evolved during the process are plotted as a function of the CO equilibrium pressure (p_{CO}), expressed in Torr (1 Torr = 133.3 Pa).

In this particular case, the first (1st) and second (2nd) run isotherms are virtually coincident indicating that CO adsorption was entirely reversible upon evacuation of the CO equilibrium pressure. For the experimental and samples details *vide infra* Sect. 1.4. It is here only recalled that the 2nd run isotherms were performed after the overnight outgassing of the reversible adsorbed phase. The isotherms experimental points were interpolated by the Langmuir model equation (*vide infra*).

As an example of the influence of the adsorption temperature, the equilibrium data for water (H_2O) adsorbed at $T = 303$, 353 and 423 K on a H-BEA zeolite specimen (outgassed at $T = 873$ K) are illustrated in Fig. 1.6. In Fig. 1.6a the three volumetric isotherms are reported (for experimental and samples details *vide infra* Sect. 1.4): as far as the equilibrium pressure p_{H2O} increases, the adsorbed amounts also increase more or less steeply according to the adsorption temperature. In Fig. 1.6b the amounts adsorbed at a constant equilibrium pressure ($p_{H2O} = 6$ Torr) are plotted against the adsorption temperature giving rise to an adsorption isobar (n_{ads} vs. T_{ads}). Note that

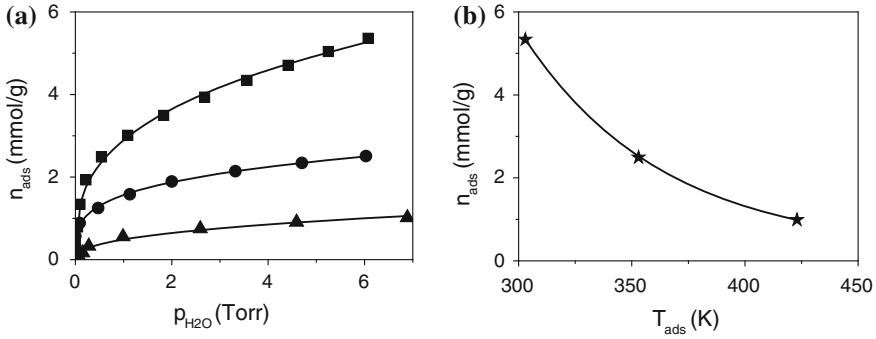

Fig. 1.6 **a** 1st run adsorption volumetric isotherms of H_2O on H-BEA zeolite at $T = 303\,K$ (*square*), $T = 353\,K$ (*circle*) and at $T = 423\,K$ (*triangle*). Experimental points interpolated by the Freundlich equation (*vide infra*). **b** Adsorption isobar (n_{ads} vs. T_{ads}) at constant $p_{H2O} = 6$ Torr; best fitting by exponential decay

in this case the adsorption process was depressed by the increasing temperature, according to the enhanced mobility of the adsorptive molecules. In all isotherms, the experimental points were interpolated by using the Freundlich isotherm equation (*vide infra*).

The isotherm experimental points can be interpolated by a variety of equations according to the mechanism of the adsorption process, which in turn depends on the nature of the gas/solid interaction. Among the different equations proposed to describe quantitatively the isotherms, the only one based on a physical model is the Langmuir equation [1, 2, 30, 32, 46].

The Langmuir model assumes a dynamic equilibrium at constant T between the gas (at pressure p) and the adsorbed layer, and requires a number of well-defined conditions: (i) the adsorption, which is limited to a monolayer, takes place at a surface consisting of a distribution of energetically equivalent, non-interacting sites; (ii) the ability of a molecule to bind at a site is independent of whether or not a nearby site is occupied (absence of lateral interactions); (iii) once adsorbed, the molecules are localized in that the activation barrier hindering migration to an adjacent site is supposed to be much larger than kT; (iv) the enthalpy of adsorption $\Delta_a H$ (per site) is constant with θ.

The Langmuir adsorption isotherm is derived from a kinetic mechanism. Let us assume for sake of simplicity that the molecule M is adsorbed molecularly (i.e. without rupture/formation of chemical bonds) from the gas at a surface site S. The fractional monolayer coverage of the sites occupied by adsorbate molecules is $\theta = \frac{N_S}{N}$. The rate of adsorption is given by the Eq. 1.1:

$$\text{adsorption rate} = k_a p\,(1 - \theta) \tag{1.1}$$

k_a being the rate constant for the adsorption and $(1 - \theta)$ the fractional monolayer coverage of sites not occupied yet by the adsorbate molecules.

The rate of desorption, k_d being the rate constant for desorption, is given by the Eq. 1.2:

$$\text{desorption rate} = k_d\theta \tag{1.2}$$

When the dynamic equilibrium is reached (adsorption rate = desorption rate) the Eq. 1.3 is obtained:

$$k_a p\,(1-\theta) = k_d\theta \tag{1.3}$$

Equation 1.4 represents the Langmuir equation:

$$\frac{\theta}{1-\theta} = \mathrm{K}p \tag{1.4}$$

Note that the constant K is obtained by the ratio of the rate constant for adsorption over the rate constant for desorption $\left(\frac{k_a}{k_d}\right)$.

The Langmuir equation is often written as reported by the Eq. 1.5

$$\theta = \frac{V}{V_{mon}} = \frac{Kp}{(1+Kp)} \tag{1.5}$$

The term V represents the adsorbate volume and V_{mon} the monolayer volume, i.e. the volume of adsorbate required to complete the monolayer.

At very low pressure the equation reduces to a linear dependence of the coverage upon the equilibrium pressure ($\theta = hp$). Conversely, at high pressure the equation reduces to the case of coverage approaching the monolayer ($\theta \approx 1$).

The monolayer coverage (V_{mon}) is hardly determined experimentally with accuracy. So, for practical purposes the Langmuir equation is suitably transformed in the so-called reciprocal linear form, as illustrated by the Eq. 1.6:

$$\left(\frac{1}{V}\right) = \frac{1}{KV_{mon}}\left(\frac{1}{p}\right) + \frac{1}{V_{mon}} \tag{1.6}$$

For isotherms obeying the Langmuir model, the reciprocal volume $\left(\frac{1}{V}\right)$ against reciprocal pressure $\left(\frac{1}{p}\right)$ plot is linear (Langmuir-type isotherms). Conversely, if the experimental data plot is not linear, Langmuir equation does not hold in describing the given adsorption process.

The monolayer capacity is obtained from the intercept $i = \frac{1}{V_{mon}}$ of the straight line. Once determined V_{mon}, the equilibrium constant K is obtained by the slope $s = \frac{1}{KV_{mon}}$ of the plot.

The monolayer volume and the equilibrium constant are typical of the adsorbent/adsorbate pairs at a given temperature. In particular, the value of K is bound to the strength of the adsorbent-adsorbate interaction: high values of K indicate large strength, low values little strength.

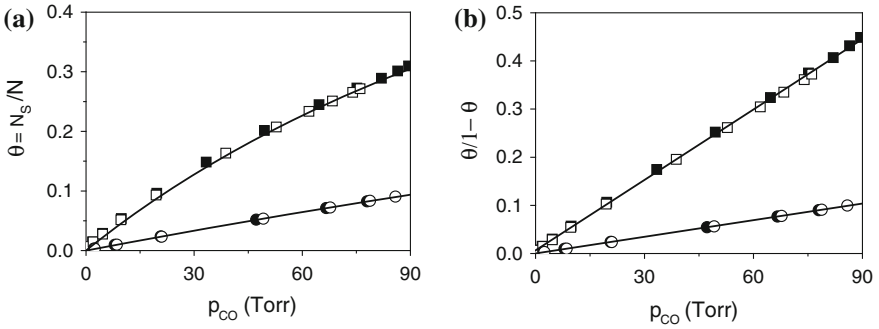

Fig. 1.7 Adsorption of CO at $T = 303\,\mathrm{K}$ on dehydrated zeolites Na–MFI (*square*) and K–MFI (*circle*). *Solid symbols* 1st run, *open symbols* 2nd run of adsorption. **a** θ_p versus p_{CO} plot. **b** $\frac{\theta}{1-\theta}$ *versus* p_{CO} plot

In the following, the very simple case of CO adsorbed at $T = 303\,\mathrm{K}$ on dehydrated Na− and K−MFI will be discussed (*vide supra* in Fig. 1.5 the experimental volumetric and calorimetric isotherms). The number of CO molecules adsorbed per gram of zeolite at p_{CO} represents the number of occupied sites (N_S), whereas the number of charge-balancing cations exposed per gram of zeolite represents the total available sites (N).

In Fig. 1.7, the coverage $\theta = \frac{N_S}{N}$ (Fig. 1.7a) and the $\frac{\theta}{1-\theta}$ quantity (Fig. 1.7b) are plotted against p_{CO}. The slope of the $\frac{\theta}{1-\theta}$ versus p_{CO} plot is the Langmuir constant K (see Eq. 1.4).

CO is a soft Lewis base which is easily polarized by the electrostatic field generated by the extra-framework alkaline-metal cations located in the MFI zeolite nanocavities. As a consequence, it is reversibly taken up by the surface when put in contact with the activated zeolite [23].

The equilibrium constant K for Na–MFI ($4.88 \pm 0.02\ 10^{-3}$ Torr^{-1}) is larger than for K–MFI ($1.15 \pm 0.02\ 10^{-3}$ Torr^{-1}), in agreement with the different polarizing power of the cations. In fact, the local electric field generated by the coordinatively unsaturated (*cus*) cations depends on the charge/ionic radius ratio, which is larger for Na^+ than for K^+, the ionic radius of the former being 0.97 Å and that of the latter 1.33 Å [47]. Note also that, according to the charge/ionic radius ratio, the maximum coverage attained at $p_{CO} = 90$ Torr was larger for Na–MFI ($\theta \approx 0.3$) than for K–MFI ($\theta \approx 0.1$).

The standard free energy $\Delta_a G^\circ$ for CO adsorption at the two alkaline-metal sites is obtained by the Langmuir equilibrium constant K by employing the Eq. 1.7:

$$\Delta_a G^\circ = -RT \ln K \tag{1.7}$$

In both cases the adsorption process in standard conditions is endoergonic, being $\Delta_a G^\circ = +13.4\,\mathrm{kJ\ mol^{-1}}$ for Na−MFI and $+17.0\,\mathrm{kJ\ mol^{-1}}$ for K−MFI. The endoergonic character of the process is witnessed by the non-spontaneity of the adsorption

unless a CO pressure is applied. In fact, by evacuating the CO pressure, the electrostatic $Na^+ \cdots CO$ and $K^+ \cdots CO$ adspecies are completely destroyed, as confirmed by the overlap of the 1st and 2nd run of adsorption (see Figs. 1.5 and 1.7).

From $\Delta_a G^\circ$ the standard entropy of adsorption $\Delta_a S^\circ$ is obtained, if $\Delta_a H^\circ$ is known. The CO adsorption enthalpy change was measured calorimetrically during the same experiments in which the adsorbed amounts were measured (*vide infra*, Sect. 1.4.2.3). We will come back to this point and to the evaluation of the $\Delta_a S^\circ$ in the section devoted to the entropy of adsorption (*vide infra*, Sect. 1.5.3).

Deviations from the Langmuir model are often observed in real systems. The Langmuir model assumptions listed above are indeed very limitative and severe: (i) the solid surface is rarely uniform: there are always "imperfections" at the surface, (ii) the mechanism of adsorption is not the same for the first molecules as for the last to adsorb. When two or more kind of sites characterized by different adsorption energies are present at the surface (as stated in point i), and when lateral interactions among adsorbed species occur (as stated in point ii), the equivalence/independence of adsorption sites assumption fails. The most energetic sites are expected to be occupied first, and the adsorption enthalpy $\Delta_a H$ (per site) instead of keeping a constant, coverage-independent value, exhibits a declining trend as far as the coverage θ increases.

Further, the adsorbed molecules are not necessarily inert, and on the top of the monolayer other molecules may adsorb and multi-layers build up: this is properly described by the Brunauer, Emmet and Teller (BET) model [2, 30, 32].

Freundlich and Temkin isotherms, which refer to the case of the adsorption at surfaces characterized by a heterogeneous distribution of active sites, will be discussed briefly [30].

Freundlich isotherm is mathematically expressed by the Eq. 1.8:

$$V_{ads} = kp^{1/n} \tag{1.8}$$

This is a purely empirical formula, where the term V_{ads} represents the adsorbed amount, p the adsorptive pressure, whereas k and n are suitable empirical constants for a given adsorbent-adsorbate pair at temperature T. The adsorbed amount are normalized either to the mass of the adsorbent or to the exposed surface area. As an example see. Fig. 1.6a, where the adsorption volumetric isotherms of H_2O on H−BEA zeolite are reported: the experimental points were interpolated by the Freundlich isotherm equation. The Freundlich isotherm assumes that the adsorption enthalpy $\Delta_a H$ (per site) varies exponentially with increasing equilibrium pressure. In fact, the experimental points in the correspondent heat of adsorption versus coverage plot were properly interpolated by an exponential fitting, as illustrated in Fig. 1.15 (*vide infra* Sect. 1.4.2.3).

Temkin isotherm is mathematically expressed by the Eq. 1.9:

$$V_{ads} = k_1 \ln (k_2 p) \tag{1.9}$$

Temkin equation too is a purely empirical formula, where V_{ads} represents the adsorbed amount and p the adsorptive pressure; k_1 and k_2 are suitable empirical constants for a given adsorbent-adsorbate pair at temperature T. Also in this case, the adsorbed amount are normalized either to the mass of the adsorbent or to the exposed surface area.

The Temkin isotherm assumes that the adsorption enthalpy $\Delta_a H$ (per site) decreases linearly upon increasing coverage. Examples of heats of adsorption decreasing linearly with coverage are reported in the literature, as for instance in the case of NH_3 adsorbed on hydroxylated silica, either crystalline, [48] or amorphous, [49] as well as in the case of CH_3OH adsorption on silica-based materials [26].

Further, it is worth noticing that at sufficiently low pressure all adsorption isotherms are linear and may be regarded as obeying the Henry's law, which is reported in Eq. 1.10:

$$V_{ads} = h\, p \tag{1.10}$$

The Henry constant h is typical of the individual adsorbate-adsorbent pair, and is obtained by the slope of the straight line representing the isotherm at low coverage.

The isotherms classification, which is of high merit in terms of generality, deals with ideal cases which in practical work are rarely encountered. In fact, most often the adsorption process over the whole interval of pressure is described by an experimental isotherm which does not fit into the classification. Nonetheless, each of the equations described above may be used over restricted ranges of equilibrium pressure, so allowing to describe the experimental isotherm through the combination of individual components to the process. In such a way the surface properties of the solid, and the thermodynamics features of processes taking place at the interface can be quantitatively described [30].

As an example, it is here mentioned that the adsorption NH_3 on a highly dehydrated silica specimen was satisfactorily described by the combination of the Langmuir and Henry isotherms. The former accounted for H−bonding interactions on isolated silanols (Si-OH), whereas the latter accounted for the aspecific adsorption on dehydrated patches of the surface, dominated by dispersion forces interactions [28].

1.4 Adsorption Microcalorimetry

The measurement of the heat of adsorption by a suitable calorimeter is the most reliable method for evaluating the strength of adsorption (either physical or chemical). Tian-Calvet heat-flow microcalorimeters are an example of high sensitivity apparatus which are suitably adapted to the study of gas-solid interactions when connected to sensitive volumetric systems [10–14, 50–55]. Volumetric-calorimetric data reported in the following were measured by means of either a C-80 or MS standard heat-flow microcalorimeter (both by Setaram, F), connected to a high vacuum (residual pressure

$p \leq 10^{-5}$ Torr) gas-volumetric glass apparatus. During the same experiment, both integral heats evolved and adsorbed amounts were measured for small increments of the adsorptive, from the gas or vapor phase. Two identical calorimetric vessels, one containing the sample under investigation, the other (usually empty) serving as reference element were connected in opposition. Thanks to the differential construction of the apparatus, all parasitic phenomena (i.e., all thermal effects other than the one due to the interaction of the gas with the solid surface) were successfully compensated. C-80 microcalorimeters allow the heats of adsorption to be measured at constant T in the room temperature -573 K range, whereas MS standard microcalorimeters in the room temperature -473 K range. The adsorptive pressure in the measurements were monitored by either a Varian Ceramicell or a Baratron MKS transducer gauge ($0-100$ Torr).

A well-established stepwise procedure was followed [16, 23, 25, 56]. Small successive doses of the adsorptive were admitted and left in contact with the adsorbent until the thermal equilibrium was attained. The 1st run of adsorption performed on the activated sample (pretreated in high vacuum conditions and/or in controlled atmosphere) will be hereafter referred to as ads. I. At any individual dose of gas introduced in the system, the evolved heat ΔQ^{int} was measured within the calorimetric cells, while the adsorbed amount Δn_{ads} was measured by volumetry. Ads. I was followed by a desorption run (des. I), performed by simple evacuation of the cell. In such a way the reversibly adsorbed phase was desorbed and either the pristine surface was restored, in case of an entirely reversible adsorption, or the pristine surface was not recovered, in case of a (partially) irreversible adsorption. Ads. II was subsequently performed in order to assess which fraction (if any) of the pristine surface sites was irreversibly occupied by the adsorbed phase (in the adopted conditions). By subtracting the ads. II curve from the ads. I one, the adsorbed fraction not removed by evacuation is evaluated. The ads. II component will be hereafter referred to as the reversible adsorbed phase, whereas the (ads. I - ads. II) component will be referred to as the irreversible phase (in the adopted conditions). Subsequent runs of adsorption (ads. III, IV etc.) are performed in some cases, if the irreversible modification of the surface is expected/suspected not to be extinguished during the ads. I [21, 23, 26]. Adsorption measurements are usually performed at least twice on a virgin portion of the same batch of the material, activated in the same conditions, to check the experiments reproducibility. The routinely run protocol of adsorption-desorption-adsorption cycles is schematically illustrated in Fig. 1.8.

1.4.1 Materials

Before illustrating an instructive selection of experimental data obtained by the method described above, it is worth doing to report a brief description of the investigated materials. Some data have been already published (as will be reported), other are original.

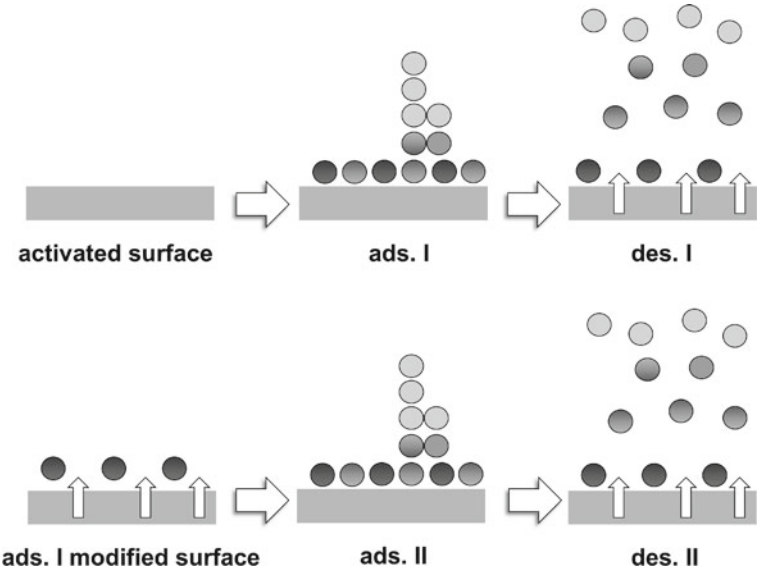

Fig. 1.8 Schematic illustration of the adsorption-desorption-adsorption cycle routinely run in order to collect the equilibrium data (evolved heats and adsorbed amounts) which are measured within the calorimetric cells at increasing equilibrium pressure

1.4.1.1 Solid Materials

H-BEA (H-BETA): a proton exchanged BEA zeolite specimen, characterized by a three-dimensional network of pores consisting of three families of 12-ring interconnected channels [57]. The specimen here illustrated was characterized by a silica-to-alumina ratio $\frac{SiO_2}{Al_2O_3} = 4.9$, corresponding to a distribution of Al atoms per unit cell $\frac{Al}{uc} = 5.9$ (see Ref. [25]. The acidic strength of such material is related to the presence of both Brønsted and Lewis acidic sites. Such latter kind of sites gives H−BEA zeolites unique catalytic properties [58–60].

BEA (BETA): an all-silica BEA zeolite specimen, characterized by the same three-dimensional network as H−BEA, but virtually free of Al species in that the silica-to-alumina ratio was $\frac{SiO_2}{Al_2O_3} = 255$, corresponding to a negligible distribution of Al atoms per unit cell $\frac{Al}{uc} \ll 0.1$ (see Ref. [25, 61]).

Prior to the adsorption experiments, H−BEA sample was outgassed for 2 h at $T = 873$ K, a temperature which ensured a maximum surface dehydration, still compatible with the stability of the structure, and yielding the maximum density of Brønsted and Lewis acidic sites. For the all-silica specimen, which was less hydrophilic than the proton-exchanged counterpart, a 2h-outgassing at $T = 673$ K was sufficient to get rid of all adsorbed water, so yielding the maximum density of Si−OH hydroxyl nests.

H−MFI (H−ZSM5): a proton exchanged MFI zeolite specimen, characterized by a three-dimensional network of pores consisting of sinusoidal and intersecting straight 10-ring channels [35]. The specimen here illustrated was characterized by a silica-to-alumina ratio $\frac{SiO_2}{Al_2O_3} = 7.5$, corresponding to a distribution of Al atoms per unit cell $\frac{Al}{uc} = 6.0$, very close to that of the H-BEA specimen illustrated above [25].

The acidic strength of H–MFI materials is related to the presence of Brønsted acidic sites whereas, opposite to H-BEA zeolites, Lewis acidic sites represent only a minor feature.

MFI–Silicalite: a Na- and Al-free defective all-silica MFI specimen, characterized by the same three-dimensional network as H–MFI, but with an extremely large silica-to-alumina ratio $\frac{SiO_2}{Al_2O_3} \rightarrow \infty$. See Ref. [25] for details.

The all-silica zeolites, both BEA and MFI, are in general characterized by a variable amount of internal defects consisting of hydroxyl nests made up of H–bonding interacting Si-OH species, located within the zeolite nanopores. A virtually perfect (i.e. defect-free) MFI–Silicalite was also investigated for comparison purposes. See Ref. [24] and references therein for details on both defective and perfect all-silica specimens.

Prior to the adsorption experiments, both H–MFI and MFI samples were outgassed for 2 h at $T = 673\,K$ in order to achieve the maximum dehydration of the surface compatible with the stability of the structure and yielding the maximum density of Brønsted acidic sites in H–MFI and of polar Si-OH hydroxyl nests in MFI–Silicalite.

Me(I)−MFI (Me(I)−ZSM5): cation-exchanged zeolites (MFI) with Me(I) = Cu^+ or Ag^+ (both belonging to the *group 11* of transition metals), or Me(I) = Na^+ or K^+ (both belonging to the *group 1* of alkaline-metals) as extra-framework species. The samples were prepared starting from the same NH_4–MFI precursor (characterized by a silica-to-alumina ratio $\frac{SiO_2}{Al_2O_3} = 7$) either by conventional wet exchange (Ag(I)−, Na− and K−MFI), or by direct CuCl gas phase exchange (Cu(I)−MFI). In all cases a nearly total exchange of the parent material extra-framework cations was achieved, as confirmed by IR spectroscopy: one Me(I) cation for every framework Al atom was present in all examined materials. For samples details see Ref. [21, 23, 62]

TiO_2 : (a) a crystallographic pure anatase obtained by a sulphate preparation and thoroughly freed from sulphate impurities, following the preparation route described in Ref. [63]; (b) the same crystallographic pure anatase but still carrying sulphate surface impurities (4–5 % SO_4 by weight) [64]. Prior to the adsorption experiments all samples were outgassed at $T = 673\,K$ for 2 h, in order to dehydrate the surface and yield the maximum density of Lewis acidic sites (i.e. *cus* Ti^{4+} cations). After outgassing, the samples were contacted at the same temperature with ≈100 Torr of O_2 for 10 min to ensure stoichiometry.

A Ca-modified silica (8% mol CaO) was obtained by adding dosed amounts of an aqueous solution of $Ca(NO_3)_2{\cdot}4H_2O$ to a dry amorphous nonporous silica (Aerosil 200 from Degussa, Frankfurt A.M., D) using the incipient-wetness impregnation technique described in Refs. [26, 65] Prior to the adsorption experiments the sample was outgassed at $T = 423\,K$ for 2 h, in order to get rid of physically adsorbed water but

without inducing any appreciable surface dehydroxylation. The choice of a vacuum activation temperature only slightly higher than room temperature was determined by the need to study the surface properties of still highly hydrated samples (i.e. of solids taken under conditions not too far from those experienced by biomaterials in contact with the biological medium).

1.4.1.2 Molecular Probes

CO specpure from either Matheson or Praxair was used as a molecular probe in order to assess the Lewis acidic properties of coordinatively unsaturated (*cus*) cations either located in the dehydrated zeolite nanocavities as charge-balancing cations, or exposed at the dehydrated surface of oxidic materials. CO is capable of interacting with the *cus* cations leading to the formation of adducts of different stability according to the chemical nature of the cation. Weak electrostatic adducts are formed on alkaline metal cations, σ-coordinated species of intermediate stability on non d/d^0 metal cations, whereas high-stability carbonyl-like species originated by a σ-coordination $+\pi$-back donation of d electrons are formed on d block metal cations.

H_2O_{vap} was used as a molecular probe to assess the hydrophilic and/or hydrophobic features of protonic (H−BEA) and all-silica (BEA) zeolites. Water (from Millipore) was distilled several times in vacuo and rendered gas-free by several 'freeze-pump-thaw' cycles. The vapor pressure of H_2O at $T = 303\,K$ is 31.8 Torr, and the standard molar enthalpy of liquefaction (i.e. the latent heat of liquefaction, q_L) is $-\Delta_L H^\circ = 44\,kJ\,mol^{-1}$.

NH_3 gas (from Praxair) was used as molecular probe of moderate basic strength (PA $= 854\,kJ\,mol^{-1}$), [66]. in order to characterize the acidic strength of Brønsted (and Lewis, if any) acidic sites in protonic and all-silica zeolites.

CH_3OH vapor, obtained by distilling in vacuo liquid methanol (Sigma-Aldrich), was rendered gas-free by several "freeze-pump-thaw" cycles. The vapor pressure of CH_3OH at $T = 303\,K$ is 164 Torr, and the standard molar enthalpy of liquefaction (i.e. the latent heat of liquefaction, q_L) is $-\Delta_L H^\circ = 38\,kJ\,mol^{-1}$.

1.4.2 Equilibrium Data

1.4.2.1 Volumetric and Calorimetric Isotherms

Adsorbed amounts and integral heat evolved will be suitably reported as a function of the increasing equilibrium pressure, i.e. as volumetric and calorimetric isotherms, respectively. Adsorbed amounts $n_{ads} = \sum \Delta n_{ads}$ were obtained by adding the individual doses amounts, Δn_{ads}, and will be reported either as mol per unit mass (mol g^{-1}) or per unit surface area (mol m^{-2}), or as molecules per square nanometer. In zeolites, in order to compare from a structural point of view the affinity of different zeolites towards the given adsorptive, the adsorbed amounts will be more suitably

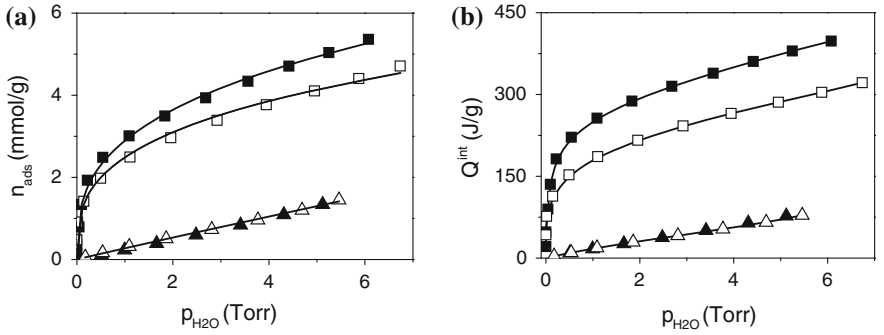

Fig. 1.9 Adsorption of H_2O_{vap} adsorbed at $T = 303\,K$ on proton-exchanged (H-BEA, square) and all-silica (BEA, up triangle) zeolites pre-outgassed at $T = 873$ and $673\,K$, respectively. **a** Volumetric isotherms. **b** Calorimetric isotherms. *Solid symbols* ads. I; *open symbols* ads. II. Adapted from Ref. [25] Fig.4

reported as molecules per unit cell (uc) or per Al atom. Integral heats $Q^{int} = \sum \Delta Q^{int}$ were obtained by adding the individual doses evolved heats, ΔQ^{int}, and will be reported per gram (J g^{-1}) or per unit surface area (J m^{-2}) of the adsorbent. Integral heats plotted as a function of the adsorbed amounts will be referred to as the integral heat curve: Q^{int} *versus* n_{ads}.

A selection of adsorption isotherms obtained for a variety of materials and probe molecules will be illustrated. Note that all the adsorption measurements reported in the following were performed at $T = 303\,K$.

H_2O_{vap} *adsorbed on* H–BEA *and all-silica BEA zeolites*. In Fig. 1.9, ads. I and ads. II volumetric (section a) and calorimetric (section b) isotherms of H_2O_{vap} adsorbed on proton-exchanged (H–BEA) and all-silica (BEA) zeolites are reported. In H−BEA an irreversible adsorption component was revealed by the non-coincidence of the ads. I and ads. II isotherms (both volumetric and calorimetric). Conversely, in the all-silica case the process was entirely reversible upon evacuation of the vapor phase, as witnessed by the coincidence of ads. I and ads. II isotherms. The isotherms experimental points were interpolated by the Freundlich equation.

H−BEA exhibited, as expected, a much higher affinity towards H_2O than the Al−free systems, owing to the presence of $Si(OH)^+Al^-$ species, characteristic of proton-exchanged zeolites and acting as Brønsted acidic sites. Such species are located within the zeolite nanocavities and are able to adsorb guest molecules by strong H–bonding interactions, often leading to the formation of protonated species [25, 67–73]. In addition, in H−BEA zeolites structural defects acting as Lewis acidic sites (i.e. strong electron acceptors) are often present [58, 60, 74–76]. It is still under debate whether such species consist of framework trigonal Al (III) atoms, [73, 77, 78] or of extra-framework Al (III) species (EFAL) located within the pores [75, 76]. Anyway, both Lewis and Brønsted acidic sites are responsible for the formation of water complexes which are stable upon room temperature evacuation.

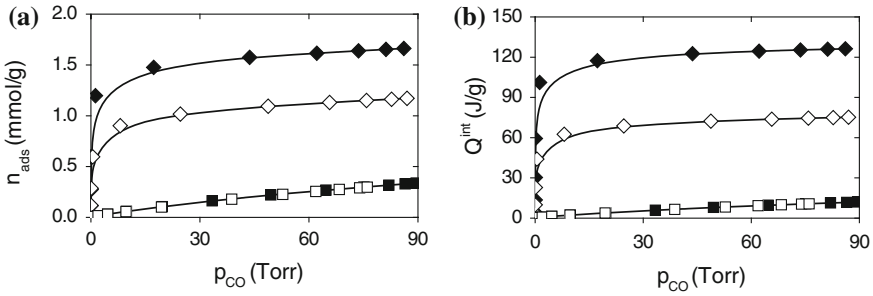

Fig. 1.10 CO adsorbed at $T = 303\,\mathrm{K}$ on zeolites Cu(I)–MFI (*diamond*) and Na–MFI (square): volumetric (**a**) and calorimetric (**b**) isotherms. Both samples were pre-outgassed at $T = 673\,\mathrm{K}$. *Solid symbol* ads. I; *open symbols* ads. II. Volumetric isotherms: adapted from Ref. [23] Fig. 3a

The affinity towards water of the all-silica counterpart was lower than that of the proton exchanged zeolite, as expected, but it was not negligible. The reported isotherms indicated that hydrophilic sites, responsible for weak and reversible water H–bonding adducts, are developed in zeolites even in the absence of framework Al atoms. Structural defects generating polar species consisting of Si−OH nests (which are characterized by a weak Brønsted acidic strength),[25, 61] are always present in Al-free zeolites, unless especially prepared in order to obtain hydrophobic, inert materials, as claimed by Flanigen et al.[36]. See also Ref. [24].

CO *adsorbed on* Me(I)-*exchanged* MFI *zeolites*. In Fig. 1.10 the ads. I and ads. II volumetric (section a) and calorimetric (section b) isotherms of CO adsorbed on Cu(I)− and Na−MFI are reported. In Fig. 1.11 ads. I and ads. II volumetric (section a) and calorimetric isotherms (section b) of CO adsorbed on Ag(I)− and K−MFI are reported. Note that the ordinate scale of the isotherms plots for Ag(I)− and K−MFI is twice as large as the Cu(I)− and Na−MFI scale, owing to the much lower adsorption capacity of the Ag(I)− and K−MFI zeolites with respect to the Cu(I)− and Na−MFI ones.

Cu(I)− and Ag(I)−MFI ads. II isotherms (both volumetric and calorimetric) lie below the ads. I correspondent isotherms, indicating the presence of irreversible phenomena. The irreversible adsorption component was quantified by taking the (ads. I – ads. II) difference in the volumetric isotherms at $p_{CO} = 90$ Torr. It was ≈30 % of total uptake (ads. I) for copper- and ≈20 % for silver-exchanged zeolites.

Conversely, in both Na− and K–MFI cases the coincidence of ads. I and ads. II isotherms confirmed the reversibility of CO adsorption. The much lower adsorption capacity witnessed by the *group 1* metal cations volumetric isotherms with respect to the two *group 11* ones is striking. The calorimetric isotherms too confirmed the much lower affinity of the former with respect to the latter. The isotherms experimental points of the *group 1* metals exchanged zeolites were interpolated by the Langmuir equation (*vide supra*, Sect. 1.3.1), whereas in the case of the *group 11* metals isotherms the curves were drawn by employing a B-Spline function, just as an aid to the eye. The two d-block metals isotherms dramatically deviate from the

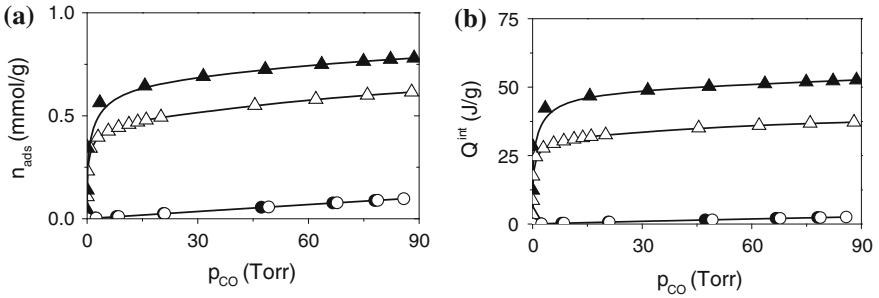

Fig. 1.11 CO adsorbed at $T = 303\,\text{K}$ on zeolites Ag(I)–MFI (*triangle*) and K–MFI (*circle*): volumetric (**a**) and calorimetric (**b**) isotherms. K–MFI was pre-outgassed at $T = 673\,\text{K}$, Ag(I)–MFI at $T = 400\,\text{K}$. *Solid symbol* ads. I; *open symbols* ads. II. Volumetric isotherms: adapted from Ref. [23], Fig. 3b

Langmuir behavior, in that in this latter case the adsorption of CO was driven by forces other than the simple electrostatic polarization, and concerns a heterogeneous distribution of active sites. In fact, Cu(I)− and Ag(I)−cations hosted in the zeolite nanocavities, besides the electrostatic polarization of CO molecule, interacted chemically with the molecule. Stable carbonyl-like species were formed at the d-block metal cations sites, through a σ-coordination of the C− end lone pair plus a partial π-back-donation of d electrons. The stoichiometry of the heterogeneous di-carbonyl $\left[\text{Cu}\,(\text{CO})_2\right]^+$ and mono-carbonyl $\left[\text{Ag}\,(\text{CO})\right]^+$ complexes was obtained from the quantitative data reported in Figs. 1.10 and 1.11. These results, confirmed also by IR spectroscopic data (see Ref. [23] and references therein for details), are in good agreement with the stoichiometry reported for the correspondent Cu(I) and Ag(I) complexes formed in homogeneous conditions [79, 80].

The differences between the two d-block metal cations can be explained on one hand from an electrostatic point of view, since the charge density of Cu(I) is much larger than that of Ag(I) cations (rCu(I) = 0.96 Å and rAg(I) = 1.26 Å) [47]. On the other hand, the overlap of the metal cations and CO orbitals in the carbonyl bond is expected to be larger for Cu(I) than for Ag(I). The adsorption of CO on Na^+ and K^+ cations hosted in the same zeolite framework allowed to roughly single out the electrostatic contribution to the two d-block metal cations/CO interaction. Na^+ and K^+ cations possess indeed a charge/radius ratio very close to that of Cu(I) and Ag(I), respectively (0.97 Å for Na^+ and 1.33 Å for K^+) [47].

NH_3 adsorbed on H−MFI and all-silica MFI zeolites. Adsorption of NH_3 has been widely used to assess the acidic strength of both Brønsted and Lewis sites at solid surfaces [68, 70, 71]. In Fig. 1.12, the ads. I and ads. II volumetric (section a) and calorimetric (section b) isotherms of NH_3 adsorbed on: (i) the proton-exchanged H−MFI zeolite, (ii) one defective MFI–Silicalite (MFI−def) and (iii) the perfect (defect-free) all-silica MFI–Silicalite (MFI−perf), are reported. In H−MFI, the adsorption was only partially reversible in agreement with the proton-transfer from the Brønsted acidic site $Si(OH)^+Al^-$ to NH_3, as reported in Ref. [81]. Conversely,

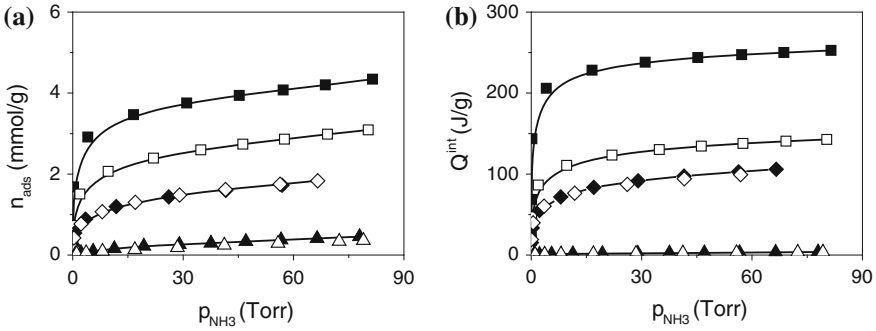

Fig. 1.12 Adsorption of NH_3 at $T = 303$ K on proton-exchanged H–MFI zeolite (*square*), defective MFI–Silicalite (MFI−def, diamond), and perfect (defect-free) MFI–Silicalite (MFI−perf, up triangle). **a** Volumetric isotherms. **b** Calorimetric isotherms. H−MFI zeolite was pre-outgassed at $T = 873$ K, MFI–Silicalite samples at $T = 673$ K. *Solid symbols* ads. I, *open symbols* ads. II

in both defective and perfect all-silica zeolites the process was entirely reversible upon evacuation of the gas phase. In this latter case NH_3 interacted only *via* hydrogen bond with Si−OH nests [24]. In the defect-free MFI–Silicalite, which exposes only unreactive siloxane bridges, the interaction was aspecific in that governed by dispersion forces due to the nanopores walls (*confinement effect*) [82–84].

1.4.2.2 Integral Heat of Adsorption

Integral heats normalized to the adsorbed amounts are referred to as the integral molar heat of adsorption at the given equilibrium pressure p: $(q_{\mathrm{mol}})_p = \left(\frac{Q^{\mathrm{int}}}{n_{ads}}\right)_p$ expressed in kJ mol^{-1}. The $(q_{\mathrm{mol}})_p$ quantity is an intrinsically average value, as it refers to the thermal response of the surface as a whole, and is comprehensive of all thermal contributions from the variety of interactions the gas molecules have experienced from the beginning of the process up to the chosen equilibrium pressure p.

By plotting the integral heats evolved against the adsorbed amounts the so-called integral heats curve is obtained (*vide infra* as an example the insets of Fig. 1.14). In the Langmuir-like adsorption characterized by a uniform distribution of equivalent, non-interacting sites the heat of adsorption is constant upon increasing coverage: the integral heats curve is thus a straight line through the origin, the slope of which gives the differential heat of adsorption (q^{diff}). In cases other than this particular one, q^{diff} is obtained by differentiating the non-linear $Q^{\mathrm{int}} = f\,(n_{ads})$ function.

The interest in dealing with differential heats stems on the fact that the differential quantities are more adequate than the average ones in describing the evolution with the increasing coverage of the adsorbate/surface sites energy of interaction.

1.4.2.3 Differential Heat of Adsorption

Differential heats of adsorption represent a reasonable measure of the energy of interaction of a (probe) molecule with the individual sites, at any adsorbate coverage. The magnitude of the heat evolved during adsorption, which depends on the nature of the adsorbate/surface sites bonding, varies upon increasing coverage as a consequence of the presence of either a heterogeneous distribution of surface sites, or lateral interactions among adsorbed species (*vide infra* Sect. 1.5.1). The shape of the q^{diff} *versus* n_{ads} plots depends on, and actually describes, the surface heterogeneity.

Differential heats of adsorption are properly defined as $q^{diff} = \frac{\delta Q^{\text{int}}}{\delta n_{ads}}$, i.e., the derivative of the $Q^{\text{int}} = f\,(n_{ads})$ function which best fits the Q^{int} *versus* n_{ads} equilibrium data.

An alternative route for evaluating q^{diff} is however first discussed here. The method is based on the use of the partial molar heats $\frac{\Delta Q^{\text{int}}}{\Delta n_{ads}}$ quantities,[10, 12, 85] i.e. the ratio of the integral heat evolved over the correspondent amount adsorbed for the individual incremental doses of the adsorptive. The $\frac{\Delta Q^{\text{int}}}{\Delta n_{ads}}$ quantity, expressed in kJ mol^{-1} is still an integral molar heat (and thus average in nature) but it refers to the thermal response of very small regions of the surface, provided that the individual doses were prepared as small as possible. Note that the limit of $\frac{\Delta Q^{\text{int}}}{\Delta n_{ads}}$ quantity for Δn_{ads} approaching zero is the true differential heat, as illustrated by the Eq. 1.11:

$$\lim_{\Delta n_{ads} \to 0} \frac{\Delta Q^{\text{int}}}{\Delta n_{ads}} = q^{diff} \tag{1.11}$$

By plotting, in the form of an histogram, $\frac{\Delta Q^{\text{int}}}{\Delta n_{ads}}$ values as a function of the adsorbed amounts n_{ads}, the evolution of the heat of adsorption upon increasing coverage is properly described. By taking the middle point of each partial molar heat $\frac{\Delta Q^{\text{int}}}{\Delta n_{ads}}$ block, the mean heat values correspondent to small portions of the surface are obtained, which represent a reasonable measure of the differential heat, as reported by several authors [10, 14, 56, 85–88].

The q^{diff} experimental points versus the n_{ads} adsorbed amounts are interpolated by functions which best fit the experimental points (*vide infra* in Fig. 1.13a the case of H_2O_{vap} adsorbed on zeolites).

For most purposes, it is convenient to define the zero-coverage differential heat of adsorption q_0, which corresponds to the energy of interaction of the molecular probe with the most energetic sites, expected to be active in the earliest stages of the adsorption process. The q_0 value is estimated by extrapolating the q^{diff} *versus* n_{ads} plot to vanishing coverage. The extrapolated quantities of experimental origin can be properly and often fruitfully compared to the computed energy of interaction of a probe molecule with an individual model site, as obtained through *ab initio* calculations [24–26, 29, 73, 89].

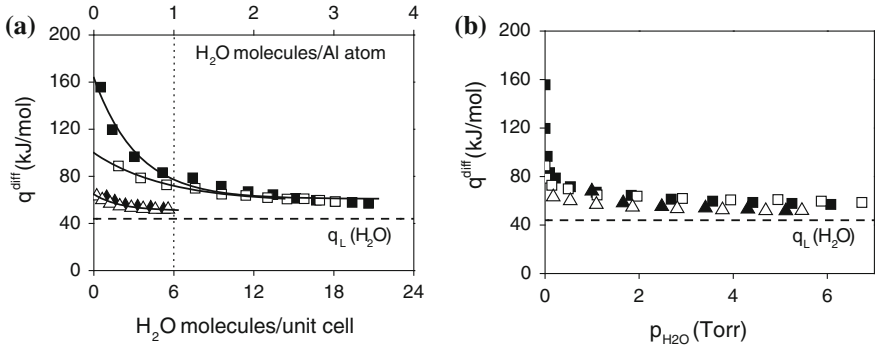

Fig. 1.13 **a** q^{diff} *versus* n_{ads} of H_2O_{vap} at $T = 303$ K on proton-exchanged (H−BEA, square) and all-silica (BEA, up triangle) zeolites, pre-outgassed at either $T = 873$ K (H−BEA) or $T = 673$ K (BEA). **b** q^{diff} *versus* p_{H2O}. *Solid symbols* ads. I; *open symbols* ads. II. Adapted from Ref. [25],Fig. 5

H_2O_{vap} adsorbed on H − BEA and BEA zeolites. In Fig. 1.13 the differential heats of adsorption of H_2O_{vap} on H−BEA and BEA zeolites are reported as a function of water adsorbed amounts (Fig. 1.13a) or water equilibrium pressure (Fig. 1.13b).

Figure 1.13a curves are the exponential functions which best fitted the partial molar heats experimental points. The q^{diff} values were plotted against the number of H_2O molecules adsorbed per unit cell, so facilitating the interpretation of the results in terms of structural features. As already outlined in describing the correspondent volumetric isotherms (*vide supra* Fig 1.9), in H−BEA case water adsorption was only partially reversible upon evacuation of p_{H_2O}. The ads. I and ads. II q^{diff} *versus* n_{ads} curves are well distinguished in the early stage of the process, namely up to the adsorption of $\approx 1 H_2O$ molecule per Al, i.e. per acidic (either Brønsted or Lewis) site. Afterwards, the two curves merge and remain constant at a heat value larger than the latent heat of liquefaction of water ($q_L = 44$ kJ mol^{-1}). The ads. I and ads. II curves for the all-silica BEA zeolite are virtually coincident and rapidly approach q_L.

In all cases, the q^{diff} *versus* n_{ads} curves are typical of heterogeneous surfaces. In H−BEA several interactions, of different strength, take place on sites of different nature located either within the zeolite nanocavities or at the external surface.

All interactions taking place simultaneously contributed to the calorimetrically measured heat, and consequently it is hard to single out the energetics of the individual contributions to the interaction. At the Brønsted $Si(OH)^+Al^-$ sites H_2O molecules are either strongly H−bonded or protonated, whereas at the Lewis acidic sites, i.e. the *cus* framework Al (III) cations, H_2O molecules are oxygen-down coordinated [25]. H_2O molecules interacted also *via* H−bonding with Si−OH nests located within the zeolite nanocavities and, more weakly, with (isolated) Si−OH species exposed at the external surface. Aspecific interactions generated by *confinement effect*,[82–84] also contributed to the overall measured heat.

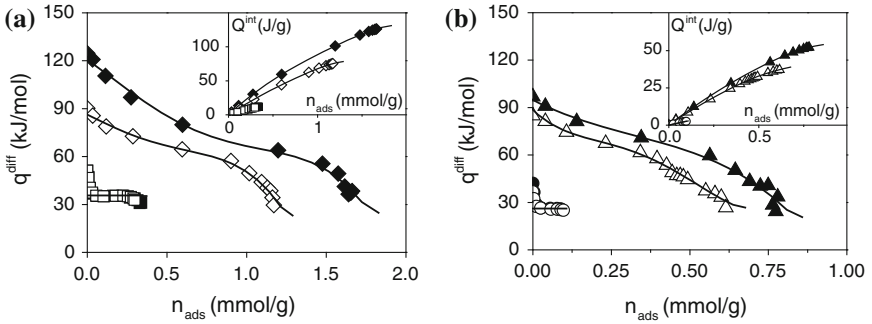

Fig. 1.14 Differential heats of adsorption versus CO uptake ($T = 303\,\mathrm{K}$). **a** zeolites Cu(I)–MFI (*diamond*) and Na–MFI (*square*). **b** zeolites Ag(I)–MFI (*triangle*) and K−MFI (*circle*). Insets: interpolated integral heats of adsorption curves Q^{int} *versus* n_{ads}. Zeolites Cu(I)−, Na− and K−MFI were pre-outgassed at $T = 673\,\mathrm{K}$, Ag(I)–MFI at $T = 400\,\mathrm{K}$. *Solid symbols:* ads. I; *open symbols* ads. II. Agreement between the experimental points (partial molar heats) and the derivative of the integral heat curves is quite good (see the text for details). Adapted from Ref. [23], Fig.4

The heats of adsorption started from a quite high zero-coverage value ($q_0 \approx 160\,\mathrm{kJ\ mol^{-1}}$), which is compatible with a chemisorption process, either the protonation of H_2O at the Brønsted acidic site or the strong oxygen-down coordination at the Lewis acidic sites. According to the *ab initio* modeling results, indicating that the H_2O/Lewis site energy of interaction is comprised in the 160-109 kJ $\mathrm{mol^{-1}}$ range (depending on the local coordination of Al (III) atom),[25] the zero-coverage heat of adsorption for H−BEA could be assigned to the H_2O/Lewis complex formation, which dominated the early stage of the adsorption. At increasing coverage the heat values decreased exponentially but remained well above the latent heat of liquefaction of water even after the adsorption of ≈4 molecules per Al atom. For one H_2O molecule adsorbed per Al atom, on average, the heat values were comprised in the $160 < q^{diff} < 80\,\mathrm{kJ\ mol^{-1}}$ range, whereas for the second-to-fourth H_2O adsorbed molecules in the $80 < q^{diff} < 60\,\mathrm{kJ\ mol^{-1}}$ range.

In the all-silica BEA specimen the zero-coverage heats of adsorption were much lower than for H–BEA ($q_0 \approx 70\ vs. 160\,\mathrm{kJ\ mol^{-1}}$, respectively) and both ads. I and ads. II curves dropped very fast down to an almost constant value, only slightly higher than $q_L = 44\,\mathrm{kJ\ mol^{-1}}$. This result indicates that, despite the absence of specific Brønsted/Lewis acidic sites, the Si−OH nests manifest a H−bonding capacity of medium strength giving to the all-silica zeolite a substantial non-hydrophobic character.

Figure 1.14b plot indicates that for adsorption leading to the same residual pressure in different runs and/or on different samples, q^{diff} values virtually coincide. Differences between the protonic H−BEA and the all-silica BEA zeolites (and between ads. I and ads. II for H−BEA) are evident at a residual pressure close to zero, at which the irreversible adsorption took place only on H−BEA.

Two examples of q^{diff} obtained by differentiating the $Q^{\mathrm{int}} = f(n_{ads})$ functions best fitting the Q^{int} *versus* n_{ads} experimental points will be discussed in the following.

CO adsorbed on Me(I)−exchanged MFI zeolites. In Fig. 1.14 the differential heat of adsorption of CO on Cu(I)− and Na−MFI (Fig. 1.14a) and on Ag(I)− and K−MFI (Fig. 1.14b) zeolites are reported as a function of the uptake. The differential heat of adsorption curves are the analytical derivative $q^{diff} = \frac{\delta Q^{\text{int}}}{\delta n_{ads}}$ of the integral heats plots which are reported in the inset of the figures. In both Cu(I)− and Ag(I)−MFI cases the integral heats curves were reasonably fitted by a polynomial of order five, whereas in the case of alkaline metal cations by a linear equation (in agreement with the Langmuirian behavior of such systems, *vide supra* Sect. 1.3.1). The experimental points reported in the q^{diff} *versus* n_{ads} plot were obtained by taking the middle points of the partial molar heats $\frac{\Delta Q^{\text{int}}}{\Delta n_{ads}}$ histogram. A reasonably good agreement exists between the two methods over the whole examined adsorption range. From both Fig. 1.14 plots it is clearly evident that at least a fraction of CO adspecies formed at the Cu(I) and Ag(I) sites are stable complexes.

The ads. I q_0 was estimated as high as ≈120 and ≈100 kJ mol^{-1} for Cu(I) and Ag(I) sites, respectively. Such values are compatible with the bond energies typical of a chemisorption process, i.e. the formation of stable carbonyl-like species. The value for the early formation of the reversible carbonyl-like species (ads. II) was lower (≈90 kJ mol^{-1}) than for ads. I and very close for the two systems. As far as the coverage increased, the heat decreased to values typical of labile species and eventually fell down to values as low as ≈35 kJ mol^{-1} for Cu(I)−MFI and ≈25 kJ mol^{-1}for Ag(I)−MFI. These latter values were ascribed to the aspecific interaction of CO with the zeolite nanopores walls. It is worth noting that the heat of adsorption associated to this interaction was much larger than the latent heat of liquefaction of CO ($q_(L) = 6$ kJ mol^{-1}).

In agreement with the Langmuir-like behavior of the Na− and K–MFI isotherms (*vide supra* Sect. 1.3.1), their Q^{int} *versus* n_{ads} curves were reasonably fitted by linear equations. A constant value for the differential heat was obtained: q^{diff} ≈35 kJ mol^{-1} for Na–MFI and ≈28 kJ mol^{-1} for K–MFI. The linear fit of the integral heat curves seemed the most realistic, in spite of the fact that in both cases at very low and at high coverage the middle points of the experimental histogram deviated from the constant value. At both low and high coverage, however, the heat values cannot be assigned to processes involving a specific $Me^+ \cdots CO$ interaction and must be disregarded in evaluating the heat of formation of the adducts. In fact, the low-coverage heterogeneity was due to the presence of a few defective centers (1–2 % of the total active sites) interacting with CO more strongly than the alkaline metal cations. Conversely, the high-coverage low heat values correspond to the aspecific interaction with the zeolite nanopores walls, similarly to what observed for Cu(I)− and Ag(I)–MFI as explained above.

NH_3 adsorbed on H−MFI and all-silica MFI zeolites. In Fig. 1.15 integral (Fig. 1.15a) and differential (Fig. 1.15b) heats of the reversible adsorption of NH_3 on a variety of defective MFI–Silicalite (Sil−A, Sil−B, Sil−C) and on a perfect (i.e. defect-free) MFI–Silicalite (Sil−D) are illustrated as a function of NH_3 uptake. Note that Sil−A and Sil−D are the same specimens as the ones named in Fig. 1.12 MFI−def and MFI−perf, respectively. See Ref.[24] for the experimental details.

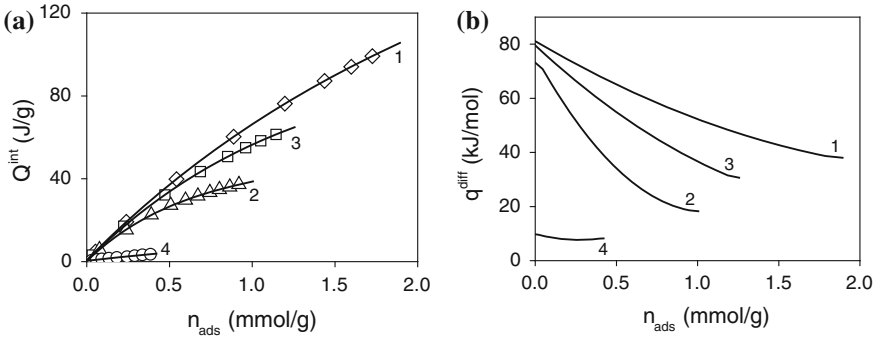

Fig. 1.15 Reversible adsorption (ads. II) of NH_3 at $T = 303\,K$ on defective MFI–Silicalite: Sil−A(*diamond*, 1), Sil-B(*up triangle*, 2), Sil−C(*square*, 3) and on perfect (i.e. defect-free) MFI–Silicalite: Sil−D(*circle*, 4). **a** Integral heats of adsorption versus NH_3 uptake. Curves interpolating the experimental points (1–4) are polynomials of order 3. **b** Differential heats of adsorption versus NH_3 uptake. Differential heats were obtained by differentiating the section (a) polynomial functions. All samples were outgassed at $T = 673\,K$. Adapted from Ref. [24] Fig. 4. Note that Sil−A and Sil−D were the same specimens as the ones named in Fig. 1.12 MFI-def and MFI-perf, respectively

The curves interpolating the integral heats plot experimental points (Fig. 1.15a) were in all cases polynomials of order 3. Differential heats reported in Fig. 1.15b were obtained by differentiating the integral heats polynomial functions. The $q^{diff} = \frac{\delta Q^{int}}{\delta n_{ads}}$ curves were all typical of heterogeneous surfaces, in that the heat values decreased upon increasing coverage, but for the perfect Silicalite (Sil−D). The defective MFI–Silicalite heat curves (Sil−A, Sil−B and Sil−C) decreased from the initial values $q_0 \approx 80$ kJ mol^{-1} down to $q \approx 20$ kJ mol^{-1}, a value close to the latent heat of liquefaction of NH_3, $q_L = 21$ kJ mol^{-1}. The evolution of q^{diff} with increasing coverage was found to vary according to the different population and/or geometrical arrangement of the polar sites (Si−OH nests) in the defective MFI–Silicalite specimens [24, 90]. Conversely, the heat of adsorption on defects-free MFI–Silicalite (Sil−D) was found to be virtually coverage-independent and assessed to a very low value ($q \approx 10$ kJ mol^{-1}), according to the lack of polar sites capable of specifically interacting with NH_3. In this latter case, the adsorption was bound to the *confinement effect* due to dispersion forces. The constant heat value, lower than latent heat of liquefaction of NH_3, could be reasonably taken as a measure of the aspecific interaction of ammonia with the siloxane surface, which takes place also at the flat surface of amorphous non-porous silica, as documented in Ref. [28].

In Fig. 1.16 the differential heat of NH_3 adsorption on one of the all-silica defective specimens discussed above (Sil−A) will be compared with the correspondent heat of adsorption on the Brønsted acidic H−MFI zeolite. Note that Sil−A will be hereafter named MFI−def, in agreement with the nomenclature of the correspondent volumetric-calorimetric isotherms illustrated in Fig. 1.12.

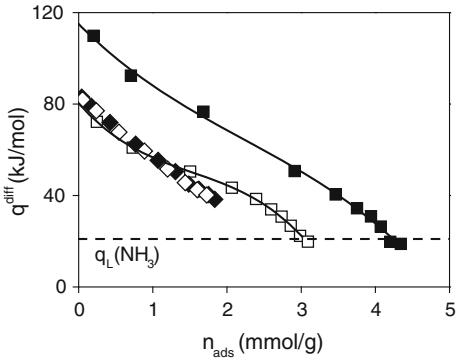

Fig. 1.16 Differential heat of adsorption versus NH_3uptake at $T = 303\,K$ on proton-exchanged H−MFI (*square*) and defective all-silica MFI−def (*diamond*) zeolites. The samples were pre-outgassed at either $T = 873\,K$ (H−MFI) or $T = 673\,K$ (MFI−def). *Solid symbols* ads. I; *open symbols* ads. II. *Solid lines*: polynomial best fitting of H−MFI ads. I and ads. II partial molar heats experimental points .

The larger affinity towards water of the Brønsted acidic H−MFI zeolite with respect to the all-silica MFI−def is well evident, as already pointed out by the Fig. 1.12 volumetric-calorimetric isotherms. The zero-coverage heat of adsorption on the proton-exchanged zeolite ($q_0 \approx 120\,kJ\ mol^{-1}$) was compatible with the proton transfer from the $Si(OH)^+Al^-$ Brønsted acidic site to the NH_3 molecule, in agreement with the standard enthalpy of NH_3 adsorption $\Delta_a H^\circ = -128 \pm 5\,kJ\ mol^{-1}$ measured as isosteric heat (*vide infra* Sect. 1.5.2) reported in Ref. [81]. Afterwards, as far as the coverage increased the H–MFI heat values decreased similarly to what observed for the all-silica MFI−def specimen, indicating that a heterogeneous distribution of surface sites was present at the surface of H−MFI as well. The contribution of the aspecific interaction with the nanopores walls (*confinement effect*) characterized by a very low heat of adsorption ($q \approx 10\,kJ\ mol^{-1}$, as measured for Sil−D/MFI−perf, see Fig. 1.15b) was most likely one of the causes for the progressive decrease of the heat of adsorption.

The H−MFI ads. II heat curve was initially virtually coincident with that correspondent to the reversible adsorption of NH_3 on the all-silica MFI−def: $q_0 \approx 80\,kJ\ mol^{-1}$. The heat values for H−MFI ads. II and for MFI−def ads. I = ads. II followed lying in a common curve up to the coverage of $\approx 1.5\,mmol\ g^{-1}$. Afterwards, the trend of the H−MFI ads. II curve changed and reached a coverage much larger than that of MFI−def.

In conclusion, the most accurate method for evaluating the differential heat depends on the specific features of the investigated systems, i.e. on the mechanism of the surface sites filling. It is worth mentioning that if the volumetric/calorimetric isotherms are properly fitted by suitable equations and if the mechanism of filling the sites is known, the q^{diff} values are obtained by processing the isotherms, as it was done in Ref. [28], dealing with the adsorption of NH_3 on a highly dehydrated

amorphous silica specimen. In that case the assumption of two independent sites was suggested/confirmed by IR spectroscopy and *ab initio* modeling: both volumetric and calorimetric isotherms were successfully simulated by the superposition of two local isotherms, one of which was Langmuir-like.

1.5 Thermodynamics of Adsorption

The adsorption of a gas at a solid surface is exothermic. This is required by the thermodynamic condition for a spontaneous process, illustrated by the Eq. 1.12:

$$\Delta_a G = \Delta_a H - T\ \Delta_a S < 0 \tag{1.12}$$

In fact, adsorption being necessarily accompanied by a decrease in entropy ($\Delta_a S < 0$) in that the degrees of freedom of the molecules in the adsorbed state are lower than in the gaseous state (*vide infra* Sect. 1.5.3 for details), it turns out that the $\Delta_a H$ term, i.e. the enthalpy change accompanying adsorption, must be negative [1, 13, 30].

Heat is not a state function and the value of the heat of adsorption depends on both the experimental conditions and the employed method of measurement. As a consequence, any physical interpretation of the experimentally determined heats of adsorption requires an accurate thermodynamic definition.

Only a few fundamental concepts will be summarized and discussed here, in that a detailed description of the thermodynamics of adsorption is out of the scopes of this Chapter. The interested reader is addressed to the exhaustive review on this subject published in 1992 by Cardona-Martinez and Dumesic [13].

Thermodynamics requires a precise and accurate use of quantities; the convention suggested by IUPAC for a proper thermodynamics nomenclature is here summarized. For any extensive quantity X we define: (i) the mean molar quantity $x = \frac{X}{n}$, which is the quantity normalized to the amount of matter expressed as moles n, and is indicated by the lower case; ii) $\frac{dX}{dn}$, the correspondent differential quantity, which is defined as the derivative of the quantity X with respect to the amount of matter expressed as moles n, and is indicated by the bar lower case: $\bar{x}$.

The quantities of interest are: (i) n, moles of adsorbate; (ii) m, mass of adsorbent; (iii) V, volume; (iv) p, pressure; (v) T, absolute temperature; (vi) R, molar ideal gas constant; (vii) A, surface area of the adsorbent; (viii) Q heat; (ix) U, internal energy; (x) H, enthalpy; (xi) S, entropy and (xii) G, Gibbs free energy. Superscripts refer to: differential quantities (d); experimentally measured quantities (exp); integral quantities (int); gas phase (g), adsorbed phase (s) and solid adsorbent (sol) quantities; standard state quantities (°). Subscript (a) refers to adsorption phenomena (e.g. $\Delta_a H$) [13, 91].

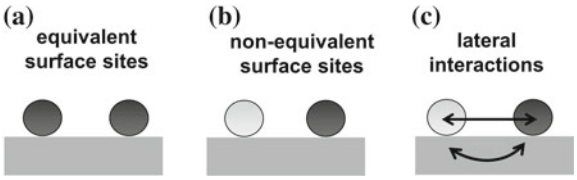

Fig. 1.17 Schematic picture of a real solid surface. Adsorption on: **a** homogeneous distribution of surface sites; **b** heterogeneous distribution of surface sites; **c** homogeneous distribution of surface sites in presence of lateral interaction among adsorbed species, either through the space or through the solid

1.5.1 Heat of Adsorption from Direct Calorimetric Methods

Heats of adsorption derived from direct calorimetric methods are based on the measurement of the heat evolved when a known amount of gas is allowed to adsorb onto a "clean" surface. A "clean" surface is a solid surface kept in high vacuum conditions after having been activated either in vacuo in order to eliminate (either totally or partially) the surface contaminants, or in controlled atmosphere/conditions.

The simplest way envisaged to perform this experiment is to measure the temperature rise in the solid. This very simple and intuitive way is of limited interest because it does not give any information about the kinetics of the heat release [10]. Further, it is worth recalling that not only the magnitude of the heat evolved during adsorption but also its variation upon increasing coverage may reveal useful information concerning the type of adsorbate/surface sites bonding, and its evolution according to the surface heterogeneity. For these reasons the equipment described above (a heat-flow Calvet-type microcalorimeter connected to a high-vacuum volumetric apparatus) is suitable for characterizing in detail the surface chemical features of a solid material. As pointed out in Sect. 1.2 (see Figs. 1.1 and 1.2), the surface of a real solid material is in general characterized by a structural and/or a chemical heterogeneity of the sites, owing to the presence of either structural defects and/or (hetero)atoms in different oxidation state. Another kind of surface heterogeneity, originated by the presence of lateral interactions among adsorbed species, is the so-called induced heterogeneity. The adsorption on either a homogeneous or a heterogeneous distribution of surface sites are schematically illustrated in Fig. 1.17a and b, respectively. Lateral interactions among adsorbed species, either through space or through solid, are envisaged in Fig. 1.17c.

In the following, the thermodynamic features of the direct calorimetric methods for measuring the heat of adsorption will be discussed. The integral heat Q^{int} is the heat evolved when n^s moles are adsorbed at constant T in a *closed gas-solid* system. Because no volume work is done, according to the First Law, the change in internal energy during the adsorption of n^s moles:

$$n^s \left(u^s - u^g\right) = n^s \Delta_a U \tag{1.13}$$

is given by the integral heat Q^{int}:

$$Q^{\text{int}} = n^s \left(u^s - u^g\right) = n^s \Delta_a U \tag{1.14}$$

and the molar integral heat of adsorption is the molar change in internal energy:

$$q^{\text{int}} = \frac{Q^{\text{int}}}{n^s} = u^s - u^g = \Delta_a U \tag{1.15}$$

Differential heat of adsorption q^d is related to the integral heat according to the Eq. 1.16:

$$q^d = \left[\frac{\delta Q^{\text{int}}}{\delta n^s}\right]_{T,A} = \Delta_a \overline{u} \tag{1.16}$$

In a *gas-solid open* system, as the one described above (i.e., a Tian-Calvet type microcalorimeter connected to a high-vacuum gas-volumetric apparatus) the system will exchange with the environment not only heat but also work and matter. Work is due to the reversible, isothermal transfer of matter to both gas ($V^g dp$) and adsorbed ($RT\ dn^s$) phase. So, the isothermal heat measured in the calorimeter at constant T is defined by the Eq. 1.17:

$$Q^{\text{exp}} = n^s \left(u^s - u^g\right) - RT\ n^s - V^g\ p \tag{1.17}$$

and is related to the molar change in internal energy by the Eq. 1.18:

$$\frac{(Q^{\text{exp}} + RT\ n^s + V^g\ p)}{n^s} = u^s - u^g = \Delta_a u \tag{1.18}$$

It turns out that the two Q^{exp} and Q^{int} quantities differ by the amount of work exchanged, as illustrated by the Eq. 1.19:

$$Q^{\text{int}} = Q^{\text{exp}} + RT\ n^s + V^g\ p \tag{1.19}$$

The differential heat of adsorption q^d, obtained by differentiating the experimental integral heats Q^{int} measured in isothermal conditions, is expressed by the Eq. 1.20:

$$q^d = \left[\frac{\delta Q^{\text{int}}}{\delta n^s}\right]_{T,A} = \left[\frac{\delta Q^{\text{exp}}}{\delta n^s}\right]_{T,A} + RT + V^g \left[\frac{\delta p}{\delta n^s}\right]_{T,A} \tag{1.20}$$

The last term in Eq. 1.20 represents either the compression work during adsorption or the expansion work during desorption, and is null when two calorimetric cells (one with the sample, the other as reference element) are connected differentially, as in the case of the equipment here described. Equation 1.20 so simplifies in Eq. 1.21:

$$q^d = \left[\frac{\delta Q^{\text{int}}}{\delta n^s}\right]_{T,A} = \left[\frac{\delta Q^{\text{exp}}}{\delta n^s}\right]_{T,A} + RT \tag{1.21}$$

which is the differential heat of adsorption at constant T and surface area A.

By combining Eqs. 1.21 and 1.18 it turns out that the change in internal energy is related to the experimental heat measured in the way illustrated by the Eq. 1.22:

$$\Delta_a U = \left[\frac{\delta Q^{\text{int}}}{\delta n^s}\right]_{T,A} = \left[\frac{\delta Q^{\text{exp}}}{\delta n^s}\right]_{T,A} + RT \tag{1.22}$$

For processes at constant pressure, we are in general more interested to the enthalpy than to the internal energy change. By considering that the condensed phases depend very little upon pressure p and that $H^s \approx U^s$, it turns out that the differential form of the enthalpy change is defined by the Eq. 1.23:

$$\Delta_a \overline{h} = \Delta_a \overline{u} - RT = \left[\frac{\delta Q^{\text{exp}}}{\delta n^s}\right]_{T,A} \tag{1.23}$$

From Eq. 1.23 it turns out that the experimental heat measured in a *gas-solid open* system, operating in a differential assembly of calorimetric cells, represents the enthalpy change associated to the adsorption. This result applies to adsorption processes performed in a *gas-solid open* system through the admission of the adsorptive on the solid material kept isothermally within a heat-flow microcalorimeter consisting of two cells in opposition.

The IUPAC nomenclature adopted in this section is not strictly followed by most Authors, as witnessed by the quoted literature and will not be followed here in describing the reported examples.

1.5.2 Heat of Adsorption from Indirect Non-Calorimetric Methods

Another classical method for determining the heat of adsorption is based on the application of the Clausius-Clapeyron equation:

$$q^{\text{st}} = RT^2 \left[\frac{\delta \ln p}{\delta T}\right]_{ns,A} = \Delta_a H \tag{1.24}$$

to a series of adsorption isotherms obtained at (at least) two different temperatures. No calorimetric measurements are needed: the heat of adsorption is evaluated by using only the equilibrium data from the isotherms. The isostere of adsorption $(p \textit{ versus } T)_\theta$ is obtained by plotting the equilibrium pressure as a function of the adsorption temperature, at constant coverage θ. The so called isosteric heat of adsorption q^{st} is determined by introducing in Eq. 1.25 (which is obtained by integrating Eq. 1.24) the

p_1 and p_2 values at T_1 and T_2, for a given constant coverage θ:

$$\ln\left(\frac{p_1}{p_2}\right) = \frac{q^{st}}{R}\left[\left(\frac{1}{T_2}\right) - \left(\frac{1}{T_1}\right)\right] \tag{1.25}$$

It is worth recalling that severe restrictions are imposed in order to obtain accurate isosteric heats data: (i) the adsorption is reversible; (ii) the gas partial molar volume is much greater than the adsorbate volume; (iii) the gas behaves ideally; (iv) the surface state does not vary during measurements; (iv) the heat of adsorption does not vary with T. For this last reason T_1 and T_2 should be as close as possible.

Dunne et al. [54] employed the Clapeyron equation for determining the isosteric heat of a variety of molecules adsorbed on Silicalite. The obtained data were compared by the same authors to the heat of adsorption measured calorimetrically by means of a home-made volumetric-calorimetric apparatus. The agreement between the two methods was fairly good.

The isotherms required to evaluate the isosteric heat may be obtained by IR spectroscopy measurements. In Ref. [92] it was demonstrated that the variable-temperature FTIR spectroscopy, with the simultaneous measurement of temperature and equilibrium pressure, may be a suitable method for obtaining the isosteric heat for an ideal Langmuir-like adsorption process. Optical isotherms of N_2 adsorption on H−ZSM5 were determined (in the 104 –183 K temperature range) from the change upon adsorption of the integrated intensity of the ν_{OH} stretching band at 3616 cm^{-1}, typical of the Brønsted acidic site $Si(OH)^+Al^-$. The adsorption enthalpy so evaluated was $\Delta_a H^\circ = -19.7 \pm 0.5$ kJ mol^{-1}, in good agreement with the calorimetric heats ($q = 19$ kJ mol^{-1}) measured at $T = 195$ K for N_2 on H−ZSM5 by Savitz et al.[93]. By the same method the standard enthalpy of adsorption of NH_3 on a H−ZSM5 zeolite was evaluated as $\Delta_a H^\circ = -128 \pm 5$ kJ mol^{-1}, [81] which is in reasonably good agreement with the zero-coverage calorimetric heat of adsorption reported in Fig. 1.16 ($q_0 \approx 120$ kJ mol^{-1}).

1.5.3 Entropy of Adsorption

In order to illustrate the role played by entropy S in adsorption processes, the entropy change $\Delta_a S$ accompanying the adsorption in a very simple case was computed, by using the standard statistical mechanics rigid rotor/harmonic oscillator formula[94]. In Fig. 1.18 the adsorption of an Ar atom at the surface of an apolar solid is schematically illustrated. The Ar atom approaches the solid surface from the gas phase: the translation entropy of the solid, which is fixed in the space, is taken as zero, whereas the free Ar atoms, before interacting with the solid surface, possess a translational entropy S_t which amounts to 150 and 170 J mol^{-1} K^{-1} at $T = 100$ and 298 K, respectively, at $p_{Ar} = 100$ Torr.

The adsorbed atom, which is not allowed to translate freely anymore, starts vibrating. Taking as reasonable vibrational frequency ≈ 100 cm^{-1}, the adsorbed atoms

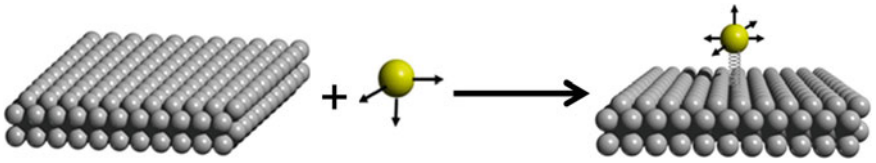

Fig. 1.18 Cartoon representing the adsorption of an Ar atom approaching a solid (apolar) surface from the gas phase

vibrational entropy is $S_v = 18$ and $43\,\mathrm{J\,mol^{-1}\,K^{-1}}$ at $p_{Ar} = 100$ Torr and at $T = 100$ and 298 K, respectively. As expected, the adsorbed atoms entropy is much lower than the free atoms entropy, and the entropy change $\Delta_a S = (S_v - S_t)$ is in all cases negative: $\Delta_a S^\circ = -132\,\mathrm{J\,mol^{-1}\,K^{-1}}$ at $T = 100\,\mathrm{K}$ and $\Delta_a S^\circ = -127\,\mathrm{J\,mol^{-1}\,K^{-1}}$ at $T = 298\,\mathrm{K}$.

This means that in a spontaneous process, which requires a negative free energy change (see Eq. 1.12), the enthalpy of adsorption must be negative in order to compensate the loss of entropy. In other words, the process must be exothermic of an amount of heat evolved at least as high as the decrease of the $T\Delta_a S$ term.

The adsorbate can be held at the surface more or less strongly and so the negative entropy change (with respect to the free molecules in the gas phase) will be more or less pronounced, according to the nature/structure of the adsorbate and to the nature and strength of the surface atoms/molecules bonds.

From a molar point of view, the term entropy of adsorption covers a great number of different functions and it is required to specify whether the function considered is a derivative or an integral, and if it refers to an equilibrium state (p, T) or to a standard state (p°, T) [95, 96].

The integral molar entropy of adsorption is the difference between the entropy of an adsorbed mole and the entropy of the adsorptive in the ideal gas state, at given p and T. It is a mean integral quantity taken over the whole amount adsorbed and it is characteristic of a given state of equilibrium. This is distinguished by the standard integral molar entropy of adsorption, which is the entropy of one adsorbed mole with respect to the entropy of the adsorptive in the ideal gas state at the same T, but under standard pressure.

It is worth recalling that the entropy of adsorption may be obtained from calorimetric experiments only if the heat exchange is reversible. A formula for evaluating the standard adsorption entropy $\Delta_a S^\circ$ from a reversible adsorption volumetric-calorimetric data was proposed by Garrone et al. [91] and applied to a selection of quasi-ideal systems, [97] consisting of CO adsorbed on non d/d^0 metal oxides, at the surface of which *cus* cations acting as Lewis acidic sites were exposed. An isothermal microcalorimeter with a discontinuous (stepwise) introduction of the adsorptive, as the one described here, was fruitfully employed.

The formation of surface Lewis complexes through a plain σ-coordination being fully reversible upon evacuation of p_{CO}, this process entirely fulfilled the requirements imposed by the method. Equation 1.26 was employed:

$$\Delta_a S = \frac{q}{T} + R - RT \ln \frac{p_{1/2}}{p^\circ} \tag{1.26}$$

In the right-hand side of the formula, the enthalpic and the ergonic contributions to the standard entropy of adsorption are recognized. The enthalpic term represented by the Eq. 1.27:

$$\Delta_a H = \frac{q}{T} + R \tag{1.27}$$

is obtained from the calorimetric data, whereas the ergonic term represented by the Eq. 1.28:

$$\Delta_a G = -RT \ln \frac{p_{1/2}}{p^\circ} \tag{1.28}$$

is obtained from the adsorption isotherms. The term $p_{1/2}$ is the equilibrium pressure at half-coverage.

The method is here applied to a very simple but instructive case: CO adsorbed *via* electrostatic polarization,[23] on Na–MFI and K–MFI pre-outgassed at $T = 673$ K. The adsorption represents in both cases an ideal process, which is characterized (within the experimental error) by a Langmuir-like behavior, as evidenced by the adsorption isotherms (*vide supra* Fig. 1.7 in Sect. 1.3.1). The calorimetric heat of adsorption was ca. 35 and 28 kJ mol^{-1} for Na–MFI and K–MFI, respectively (*vide supra* Sect. 1.4.2.3, Fig. 1.14a, b). The half-coverage equilibrium pressure (obtained by the adsorption isotherms) were $p_{1/2} = 200$ Torr for Na−MFI and 850 Torr for K−MFI. In both cases the reference state for the gas phase was $p^\circ = 1$ Torr, as done in previous work (see Ref. [18, 97]). The obtained standard adsorption entropy was $\Delta_a S^\circ = -151$ J mol^{-1} K^{-1} for Na–MFI and -140 J mol^{-1} K^{-1} for K−MFI.

Note that: (i) the loss of entropy for CO adsorbed at a polar surface through electrostatic forces was slightly larger than for the aspecific interaction of Ar atoms adsorbed at an apolar surface discussed above; (ii) the loss of entropy for CO adsorbed on Na−MFI was larger than on K−MFI, in agreement with the larger strength of adsorption of CO on Na^+ than on K^+ sites.

In the following, the evaluation of the adsorption entropy change for the slightly more complex case of CO σ-coordinated (at $T = 303$ K) on a variety of TiO_2 − anatase specimens (pre-outgassed at $T = 673$ K) will be illustrated. At the TiO_2 dehydrated surface, CO was adsorbed giving rise to two adspecies, as witnessed by two distinct IR bands located at $\nu_{CO} = 2188$ and 2206 cm^{-1}, as reported in Ref. [18] As illustrated schematically in Fig. 1.19 the two adspecies were formed on two different Lewis acidic sites made up of structurally different *cus* Ti^{4+} cations. They were named species A and B, and their spectroscopic and energetic features are summarized in the figure.

Species A ($\nu_{CO} = 2188$ cm^{-1}) were formed at the 5-coord Ti^{4+} cations typically exposed at the flat planes of anatase nanocrystals, whereas species B ($\nu_{CO} = 2206$ cm^{-1}) were formed at the 4-coord Ti^{4+} cations, which are exposed at the steps, corners and kinks of the flat planes [98]. As extensively illustrated in Ref. [18] species − A ν_{CO} moved from 2188 down to 2184 cm^{-1}as far as the

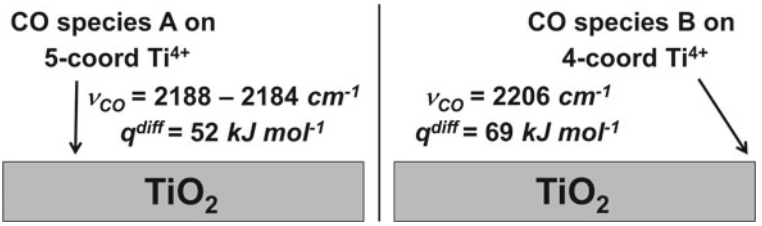

Fig. 1.19 Spectroscopic and energetic features of species A and B formed upon adsorption of CO at $T = 303$ K on TiO_2—anatase pre—outgassed at $T = 673$ K. *Left side* Species A formed on 5-coord Ti^{4+} cations exposed at the flat planes of anatase nanocrystals. *Right side* Species B formed on 4-coord Ti^{4+} cations, exposed at steps, corners and kinks of the flat planes

coverage increased, suggesting the presence of surface heterogeneity among CO adspecies. Conversely, species-B ν_{CO} remained constant at 2206 cm^{-1} at any coverage examined, suggesting that such species were formed at structurally equivalent and non-interacting sites. The heat of adsorption values were found to be coverage-independent for both species A and B: $q^{diff} \approx 52$ kJ mol^{-1} and ≈ 69 kJ mol^{-1}, respectively.

According to the constancy of both ν_{CO} spectral position and heat of adsorption, species—B adsorption was considered Langmuirian and the Eq. 1.26 could be applied straightforward. The standard molar entropy of adsorption was so evaluated from the calorimetric data ($q^{diff} \approx 69$ kJ mol^{-1}) and the Langmuir adsorption isotherm ($p_{1/2} \approx 7$ Torr), and turned out to be $\Delta_a S^\circ = -237$ J mol^{-1} K^{-1}. Note that this value is larger than both $\Delta_a S^\circ = -151$ J mol^{-1} K^{-1} and $\Delta_a S^\circ = -140$ J mol^{-1} K^{-1} obtained for the weak physical adsorption of CO on Na— and K—MFI (*vide supra*). The larger loss of entropy in the TiO_2 case with respect to the alkaline-metal exchanged zeolites was due to the stronger $Ti^{4+} \leftarrow$ CO bond, responsible for the associative chemisorption.

Conversely, as far as species A are concerned, the adsorption was found to deviate from the ideal Langmuirian behavior, as witnessed by the variation of ν_{CO} with coverage. The apparent contradiction with the constancy of the heat of adsorption was interpreted as due to the quite scarce population of sites A active towards CO at $T = 303$ K, which prevented an accurate determination of the evolution of the heat of adsorption with coverage [18].

In any case, Langmuir model did not hold in describing species—A thermodynamic features and Eq. 1.26 employed for species B did not apply. So, the entropy of CO adsorption at A sites was obtained by considering that, in the very early stage of adsorption, the coverage θ increased linearly with the p_{CO} [18]. By employing the Eq. 1.29, based on the Henry-like isotherm:

$$\Delta_a S = \frac{q}{T} + R + R \ln h \tag{1.29}$$

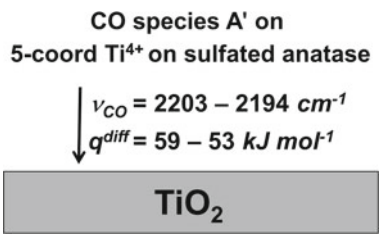

Fig. 1.20 Spectroscopic and energetic features of species formed on 5-coord cations exposed at the flat planes of dehydrated sulphated TiO_2—anatase nanocrystals

the low-coverage standard molar entropy of adsorption was evaluated from the calorimetric data ($q^{diff} \approx 52$ kJ mol^{-1}) and the Henry adsorption isotherm ($h = 0.027$ Torr^{-1}). It turned out to be $\Delta_a S^\circ = -194$ J mol^{-1} K^{-1}. This datum, which is lower than $\Delta_a S^\circ = -237$ J mol^{-1} K^{-1} obtained for species B, is in agreement with the less stronger interaction of CO with sites A with respect to sites B, which implied a lower loss of degree of freedom of the CO molecule.

The heterogeneity features of the 5-coord $Ti^{4+} \leftarrow$ CO complex were investigated in more detail on the dehydrated sulphated—TiO_2 anatase, which exhibited a population of 5-coord $Ti^{4+} \leftarrow$ CO adducts larger than that of the unsulphated specimen [18]. No B—*type* CO adspecies were formed, as witnessed by the presence of a single ν_{CO} band, initially located at 2203 cm^{-1}, as reported in Ref. [18]. The spectroscopic and energetic features of the single CO adspecies formed at the *sulphated* − TiO_2 surface, which will be named species A′, are summarized and schematically illustrated in Fig. 1.20. The presence at the surface of strong electron-withdrawing sulphate moieties caused the CO oscillators frequency to increase for sulphated anatase with respect to the unsulphated specimen (2203 cm^{-1} vs. 2188 cm^{-1}, respectively). The same occurred for the heat of adsorption which was found to increase from $q^{diff} \approx 52$ kJ mol^{-1} (unsulphated anatase) up to ≈ 59 kJ mol^{-1} (sulphated specimen). Note also that both CO stretching frequency ($\nu_{CO} = 2203 - 2194$ cm^{-1}) and heat of adsorption (59—53 kJ mol^{-1}) varied upon increasing coverage, clearly indicating the presence of induced heterogeneity among the 5-coord $Ti^{4+} \leftarrow$ CO adspecies. This datum confirmed the ability of TiO_2 to transmit electronic effects [18, 22].

The adsorption of species A′ being non-Langmuirian, Eq. 1.26 could not be applied and the low-coverage entropy change for species A′ was evaluated by employing the formula based on the Henry isotherm, with $h = 0.073$ Torr^{-1}. A value of $\Delta_a S^\circ = -208$ J mol^{-1} K^{-1} was obtained, which is larger than that obtained for species A ($\Delta_a S^\circ = -194$ J mol^{-1} K^{-1}) and lower than that obtained for species B ($\Delta_a S^\circ = -237$ J mol^{-1} K^{-1}). According to the fact that the CO entropy loss is lower when the molecule is less tightly bound, the sequence of entropy values for species A, A′ and B was in agreement with the sequence of the enthalpy values ($q^{diff} \approx 52$, 59 and 69 kJ mol^{-1}, respectively).

$\Delta_a G^\circ$ values, obtained by combining the $\Delta_a S^\circ$ and $\Delta_a H^\circ$ terms, were positive in all cases reported. The endoergonic character of the process indicated the non-spontaneity of the adsorption unless a CO pressure is applied: by evacuating the

equilibrium CO pressure, $Ti^{4+} \leftarrow CO$ complexes were completely destroyed, as confirmed by the coincidence of the 1st and 2nd run of adsorption (not reported for the sake of brevity; for details see Ref. [18]). It is worth of noticing that $\Delta_a G^\circ$ values were more positive for the weak electrostatic $Na^+ \cdots CO$ and $K^+ \cdots CO$ adducts ($\Delta_a G^\circ = +13$ and $+17\,kJ\ mol^{-1}$, respectively), than for the $Ti^{4+} \leftarrow CO$ $\sigma-$coordinated complexes ($\Delta_a G^\circ = +9$, $+7$ and $+6\,kJ\ mol^{-1}$ for A, A′ and B species, respectively), in agreement with the increased strength of the coordinative chemisorption with respect to the plain polarization of the CO molecule.

In the reported examples, an isothermal microcalorimeter with a discontinuous (stepwise) introduction of the adsorptive was fruitfully employed. An alternative, suitable way to collect the experimental data required for determining the enthalpy and entropy changes accompanying the adsorption process is to follow the procedure implying the slow-and-constant adsorptive introduction which was extensively described in Ref. [99].

The adsorption entropy of N_2 and of NH_3 on a H−MFI zeolite was evaluated starting from the correspondent optical Langmuir-like isotherms (*vide supra* Sect. 1.5.2), as reported for N_2 in Ref. [92] and for NH_3 in Ref. [81]. The entropy change was negative for both adsorptives, but much more negative for the latter ($\Delta_a S^\circ = -184 \pm 10\,J\ mol^{-1}\ K^{-1}$) than for the former adsorbate ($\Delta_a S^\circ = -125 \pm 5\,J\ mol^{-1}\ K^{-1}$), as expected on the basis of the larger adsorption strength of NH_3 than of N_2.

1.6 Adsorption of a Single Component: Physisorption Versus Chemisorption

Forces governing adsorption depend on the nature of both adsorbent and adsorptive. They are distinguished in: (i) van der Waals/London-dispersion forces, similar to the forces leading to the non-ideal behavior of gases and eventually to the formation of a liquid phase; (ii) chemical (covalent) forces leading to the formation of a true chemical bond between the adsorbate and surface atoms. In the former case the process is called physical adsorption (*physisorption*), in the latter case chemical adsorption (*chemisorption*), [2, 32]; (iii) H–bonding interactions are variably classified as responsible for either physical or chemical adsorption. In fact, H–bonding interactions originate surface complexes of variable stability according to the nature of the involved species [100].

The total potential energy of the interacting moieties is quantitatively described by the Lennard-Jones potential, [1, 2, 30, 32] which includes attractive and repulsive energy terms.

Physisorption is intrinsically weak and is characterized by heats of adsorption relatively small, close to the enthalpy of liquefaction of the adsorptive, typically comprised in the $5-45\,kJ\ mol^{-1}$ range; it is in general favored by temperatures close

to the boiling point of the adsorptive. As a consequence of the non-covalent nature of the interaction, adsorbate and adsorptive are chemically equivalent moieties.

Chemisorption, consisting of a chemical reaction confined to the solid surface, does involve rearrangement of electrons of both adsorptive molecules and surface atoms, yielding new surface terminations. Adsorptive and adsorbate being chemically different species in dissociative chemisorption, spectroscopic and/or *ab initio* modeling methods are required to assess the nature of surface species formed upon contact of the adsorptive with the reactive surface atoms [25, 26, 29]. Further, *chemisorption* is structure-sensitive in that the features of the process depend on the solid crystal structure (see for instance anatase vs. rutile, [56, 101] and amorphous silica vs. crystalline quartz, [15, 85, 102]) and on the crystal faces exposed by the solid material [103].

Chemisorption heats are generally larger than *physisorption* heats, and are typically comprised in the 80−400 kJ mol^{-1} range. Dissociative chemisorption is distinguished from associative chemisorption, which involves the coordination of the molecules as such [16, 23, 26, 29]. In this latter case, the enthalpy change is not in general as large as for dissociation: it can be even lower than ≈80 kJ mol^{-1}, as for instance for the case of CO adsorbed on *cus* non d/d^0 metal cations described above. The enthalpy change for adsorption driven by H–bonding interactions may cover a large range of values, in that the correspondent interaction energy depends in a complex way on the chemical nature of the participating atoms, as well as on the distances and angles between them. For instance, the zero-coverage enthalpy change for H_2O adsorption on hydroxylated silica, which is characterized by two H−bonds per adsorbed molecule on adjacent Si−OH terminations, is $-(\Delta_a H)_0$ ≈60 kJ mol^{-1} for amorphous silica and ≈80 kJ mol^{-1} for crystalline silica [15, 49]. This datum does suggest that (at least at low coverage) H−bonding interactions exhibit a certain degree of specificity, similarly to *chemisorption*. The energy of H−bonding interactions at the water/all-silica zeolites interface is even larger than for plain silica as indicated by a zero-coverage adsorption enthalpy of ≈100 kJ mol^{-1} [25].

Conversely, the enthalpy change for H_2O adsorption on dehydroxylated silica, which is characterized by only one H−bond per adsorbed molecule on isolated Si−OH terminations, is quite low: $-\Delta_a H < 44$ kJ mol^{-1}, and virtually surface-coverage independent [15, 56, 85].

Also CH_3OH adsorption on hydroxylated silica is structure-sensitive: on crystalline silica the H−bonding adsorption enthalpy at vanishing coverage is $-(\Delta_a H)_0$ ≈90 kJ mol^{-1},[15] whereas on amorphous silica is only ≈70 kJ mol^{-1} [26].

NH_3 is adsorbed on all-silica zeolites and on hydroxylated amorphous silica with a zero-coverage adsorption enthalpy as high as ≈80 kJ mol^{-1},[24] whereas on dehydroxylated silica $-(\Delta_a H)_0$ is only ≈60 kJ mol^{-1} [28].

In all cases, at increasing equilibrium pressure the adsorption approaches the adsorptive liquid phase, and the adsorption enthalpy approaches the adsorptive latent enthalpy of liquefaction $-\Delta_L H$, as typically occurs for physical adsorption at $\frac{p}{p^\circ} \rightarrow 1$ [28, 56, 85, 104].

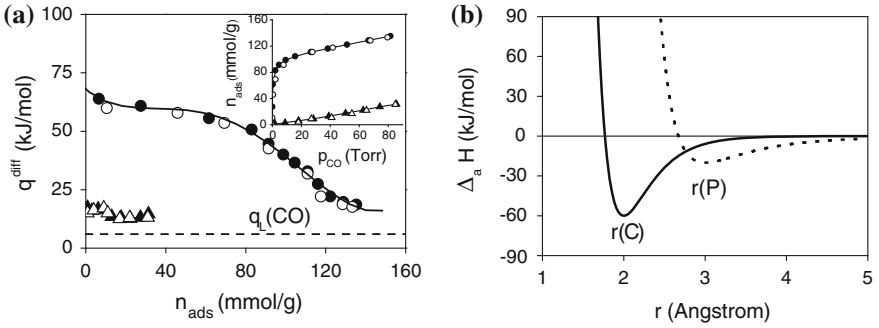

Fig. 1.21 **a** Differential heats of adsorption of CO, at $T = 303$ K, on proton-exchanged zeolite H−BEA zeolite (*circle*) and on defective MFI–Silicalite (*up triangle*) as a function of the increasing coverage. Inset: volumetric isotherms. H–BEA zeolite was pre-outgassed at $T = 873$ K, MFI–Silicalite at $T = 673$ K. *Solid symbols* ads. I, *open symbols* ads. II. *Dashed line* Latent heat of liquefaction of CO, $q_L = 6$ kJ mol^{-1}. **b** One dimension potential energy diagram for physical adsorption (*dotted line*) and associative chemical adsorption (*solid line*). See text for details

In the following, the adsorption of CO on a H−BEA zeolite specimen, characterized by both Brønsted and Lewis acidic sites (consisting these latter of structural defects in zeolite framework), will be discussed.

The room temperature adsorption of CO on protonic zeolites allowed Lewis acidic sites to be calorimetrically discriminated from the Brønsted acidic ones: Al(III) ← CO adducts of relative stability were formed at the *cus* Al(III) Lewis sites, whereas only very weak H−bonding adducts were formed at the Brønsted $Si(OH)^+Al^-$ acidic sites [73].

In Fig. 1.21a, the differential heats of adsorption of CO on H−BEA zeolite and on MFI–Silicalite are reported as a function of the adsorbed amounts. Volumetric isotherms are illustrated in the figure inset. In both cases the adsorption was fully reversible upon evacuation of the CO pressure, as typical of both physical and weak, associative chemical adsorption. For H−BEA a constant heat plateau at $q \approx 60$ kJ mol^{-1} was measured. This value is typical of a specific interaction of CO with coordinative unsaturated Al(III) atoms, as it was confirmed by combining adsorption microcalorimetry and molecular modeling [73, 74, 78, 89] Note that the heat value was close to the heat of adsorption of CO at *cus* Al(III) sites on transition catalytic alumina, a typical Lewis acidic oxide [55, 73]. Once saturated the Al(III) defects, the heat of adsorption started decreasing down to values typical of the H−bonding interaction of CO with the Brønsted acidic sites ($-\Delta_a H \approx 30$ kJ mol^{-1}, as reported by Savitz et al. [93]) and with polar defects, either confined in the zeolite nanopores or at the external surface.

Conversely, the heat of adsorption of CO at polar sites located in the all-silica nanopores (Si−OH nests) was much lower ($q \approx 17$ kJ mol^{-1}) than on H−BEA, and virtually constant over the whole coverage examined in agreement with the formation of very weak H−bonding adducts, as described in Refs. [73, 105]. The adsorption capacity of the all-silica zeolite was dramatically lower than that of the proton-exchanged zeolite, as witnessed by the correspondent isotherms reported in the inset

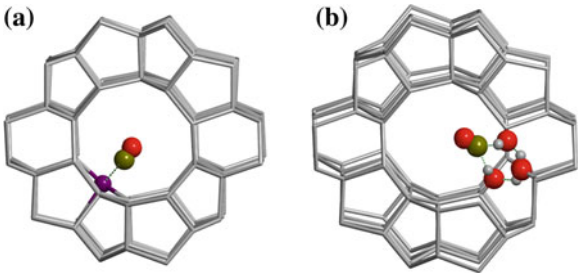

Fig. 1.22 Cartoon representing the CO adducts formed within a zeolite nanopore. **a** CO σ-coordinated on trigonal Al(III) atom (Lewis acidic site). **b** CO H−bonded at polar sites Si−OH (nests). Courtesy of Prof. Piero Ugliengo, University of Torino

of Fig. 1.21. In Fig. 1.21b a schematic one-dimension potential energy diagram is illustrated, including on one hand the CO physical adsorption on MFI–Silicalite and on the other hand the associative chemical adsorption on H−BEA. The classical Lennard-Jones formula,[2, 30, 32, 106] was used. Note that both physical and chemical adsorption of CO, which occur in different zeolites in the present example, are reported in the same plot just for comparison purposes. The right-side curve represents *physisorption*. The Si−OH nests in MFI–Silicalite are the P sites at which CO is adsorbed *via* weak H−bonding interaction and r(P) is the equilibrium separation between the two interacting moieties (in this case set to ≈3 Å). The enthalpy change $-\Delta_a H$(P) is set at ≈17 kJ mol^{-1}, according to the heat of adsorption reported in Fig. 1.21a. The left-side curve represents the enthalpy diagram for chemisorption. C are the associative-chemisorption sites at which CO is σ−coordinated, i.e. the *cus* Al(III) cations acting as Lewis acidic sites. r(C) is the equilibrium separation between the two interacting moieties (in this case set to ≈2.5Å); $-\Delta_a H$(C) is the negative enthalpy change (≈60 kJ mol^{-1}) according to the heat of adsorption plateau reported in Fig. 1.21a.

In Fig. 1.22 a cartoon illustrating the formation in a zeolite nanopore of the Al(III) ← CO complex (Fig. 1.22a) at the Lewis acidic site, and of the Si−OH· · ·CO H–bonding adduct (Fig. 1.22b) is reported.

The same kind of one-dimension potential energy diagram (not reported for the sake of brevity) can be applied to compare NH_3 interacting *via* H−bonding with polar sites (Si−OH nests) and NH_3 interacting *via* dispersion forces with the nanopore walls of an all-silica zeolite (*confinement effect*). In Fig. 1.23a the former interaction is illustrated, in Fig. 1.23b the latter one. The H−bonding interaction of NH_3 with Si−OH nests described in Fig. 1.23a cartoon is quite strong, as witnessed by the relatively high zero-coverage heat values measured for defective MFI–Silicalite (q_0 ≈80 kJ mol^{-1}, see the heat plots in Figs. 1.15b and 1.16). The process could be reasonably classified as associative chemisorption. Conversely, the aspecific interaction of NH_3 with the nanopore walls (Fig. 1.15b) is much weaker, as inferred by the adsorption heat measured for NH_3 adsorbed on defects-free MFI–Silicalite

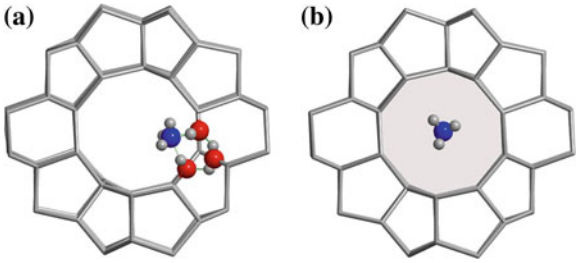

Fig. 1.23 Cartoon representing the NH_3 adducts formed within an all-silica zeolite nanopore. **a** NH_3 H−bonded at polar sites (Si−OH nests). **b** NH_3 interacting with the nanopore walls through dispersion forces. Courtesy of Prof. Piero Ugliengo, University of Torino

($q \approx 10$ kJ mol^{-1}, see Fig. 1.15b), which remained constant with increasing coverage, in that insensitive to possible surface heterogeneity.

As an example of associative/dissociative chemisorption, the interaction of CH_3OH with a Ca-modified amorphous silica specimen will be discussed. This latter material was adopted as a model system to investigate the role of Ca species in the development of bioactivity in sol-gel glasses (see Ref. [26] and references therein). The interaction involved both physical and chemical adsorption. The former process consisted of H−bonding interactions (the only ones occurring at the surface of the parent plain silica specimen, data not reported for the sake of brevity), which originated rather labile adducts on silica polar terminations and were eliminated by pumping off at the adsorption temperature. *Chemisorption* involved both associative and dissociative processes. The associative adsorption at the surface *cus* Ca^{2+} cations (acting as Lewis acidic sites), yielded coordinated CH_3OH species, a fraction of which was eliminated by evacuation of the methanol pressure at the adsorption temperature (*weak associative chemisorption*). Another fraction was eliminated only by outgassing at temperatures as high as $T = 423$ K, according to the relatively high energy of interaction, $q_0 \approx 100$ kJ mol^{-1}, measured in the early stage of the adsorption (*strong associative chemisorption*). A further fraction was found to resist outgassing up to $T > 573$ K, and was assigned to a dissociative chemical adsorption. Dissociative adsorption consisted of a chemical reaction at Ca sites, yielding $Si-OCH_3$ and Ca−OH as new surface terminations. This process was slow, slightly less exothermic than associative *chemisorption* and was found to depend on both CH_3OH pressure and contact time, as illustrated in Fig. 1.24, in which the volumetric isotherms (Fig. 1.24a) and the q^{diff} *versus* n_{ads} plots (Fig. 1.24b) are reported for a first (ads. IA and ads. IIA) and a second set of measurements (ads. IB and ads. IIB). A large difference between ads. IA and ads. IIA curves is well evident in both volumetric isotherms and heat of adsorption plots, indicating the presence of an irreversible component due to a chemical adsorption. The standard ads-des-ads protocol was followed until a fourth adsorption run without getting evidence that irreversible adsorption was extinguished. Data for the third (ads. IIIA) and the fourth (ads. IVA) runs, see Ref. [26], are not reported for the sake of brevity. The reported results indicated that the process originating irreversibly adsorbed species, consisting of both strong associative and dissociative *chemisorption*, as demonstrated by IR spectroscopy and *ab initio* modeling, [26] was not accomplished within the second adsorption (ads. IIA), as typically observed, but

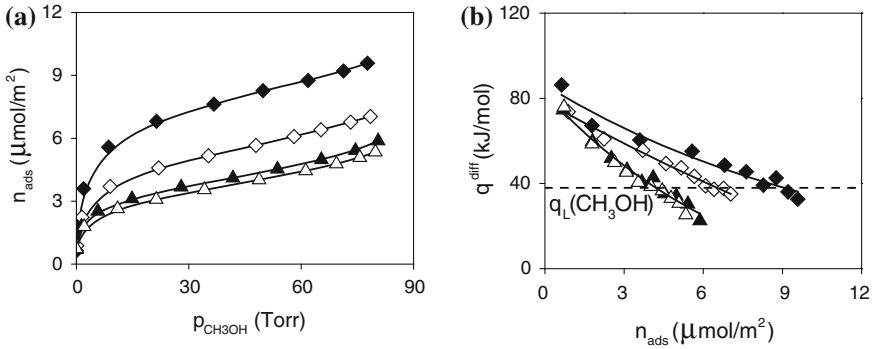

Fig. 1.24 Adsorption (at $T = 303$ K) of CH_3OH vapor on Ca–modified silica outgassed at $T = 423$ K. **a** Volumetric isotherms. **b** q^{diff} *versus* n_{ads} plots. Ads. IA: *diamond, solid symbols*; ads. IIA: diamond, *open symbols*. Ads. IB (run after evacuating overnight the sample previously kept 3 days in contact with ≈80 Torr of CH_3OH): *triangle, solid symbols*; ads. IIB: *triangle, open symbols*. Adapted from Ref. [26] Fig. 12

continued in all subsequent adsorption steps. The irreversible adsorption was found to represent a progressively decreasing component of the overall uptake, and for the fourth adsorption run became almost negligible. After the fourth adsorption the sample (still in the calorimeter at $T = 303$ K) was kept in contact with CH_3OH pressure ($p \approx 80$ Torr) for 3 days, and then it was evacuated overnight at the same temperature. A new set of ads-des-ads runs were then performed (ads. IB and ads. IIB). The presence of a new measurable irreversible component was detected, as witnessed by the non-coincidence of ads. IB and ads. IIB isotherms reported in Fig. 1.24a. This datum confirmed that the prolonged contact of the surface with a large CH_3OH pressure allowed (some of the) coordinated species to react, yielding an increased amount of $Si-OCH_3$ and $Ca-OH$ surface species. The q^{diff} *versus* n_{ads} plots reported in Fig. 1.24b were typical of highly heterogeneous surfaces, in that heat values progressively decreased with increasing coverage. The zero-coverage heat values for the first set of data were $q_0 \approx 100$ kJ mol^{-1} for ads. IA and $q_0 \approx 80$ kJ mol^{-1} for ads. IIA. The ads. IA curve crossed the heat of liquefaction of methanol line ($q_L = 38$ kJ mol^{-1}) at a CH_3OH coverage of ≈9.0 μmol m^{-2}, corresponding to ≈5.4 molecules nm^{-2}, whereas the ads. IIA curve at a CH_3OH coverage of ≈6.5 μmol m^{-2}, corresponding to ≈3.9 molecules nm^{-2}. The ads. IB and IIB curves, even starting from a q_0 value close to the of ads. IIA, decreased together much more sharply than that of ads. IA and ads. IIA and approached steeply values lower than the heat of liquefaction of methanol, already at a CH_3OH coverage of ≈4.2 μmol m^{-2}, corresponding to ≈2.5 molecules m^{-2}. IR spectroscopy data, also combined with *ab initio* calculations, confirmed a precursor-mediated kinetics, in which coordinated CH_3OH was a precursor for the methoxylation reaction [26].

In Fig. 1.25 the one-dimension potential enthalpy diagram for physical adsorption (dotted line) and for associative (dot-dashed line) and dissociative (solid line) chemical adsorption schematically illustrates the features of the interactions described

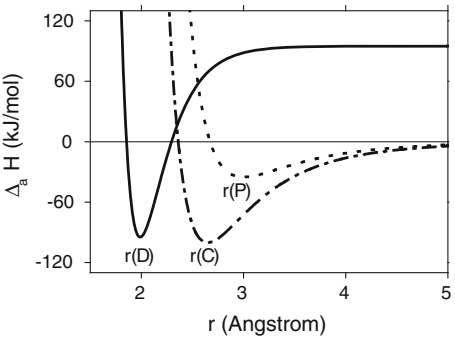

Fig. 1.25 One-dimension potential energy diagram for physical adsorption (P, *dotted line*), and for associative (C, *dashed line*) and dissociative (D, *solid line*) chemical adsorption. See text for details

above. The classical Lennard-Jones formula,[106] was used for *physisorption* and coordinative *chemisorption*, whereas a Morse expression was used for dissociative *chemisorption* [107].

The right-side curve represents physisorption. P indicates the physical adsorption site exposed at the silica matrix surface (polar terminations Si−OH) at which CH_3OH is weakly H−bonded; r (P) is the equilibrium separation between the two interacting moieties (set to ≈3Å) and $-\Delta_a H$ $(P) \approx 35\,\text{kJ mol}^{-1}$ is the enthalpy of adsorption. The left-side curves represent the enthalpy diagram for *chemisorption*. Curve C represents the coordination of CH_3OH at Ca sites (associative *chemisorption*), whereas curve D represents the methoxylation reaction of coordinated methanol (dissociative *chemisorption*). The equilibrium separation r(C) between the two interacting moieties is set to ≈2.5Å, whereas the equilibrium separation r(D) in dissociative *chemisorption* is set to ≈2.0Å, a lower value than r(C). The enthalpy of adsorption $-\Delta_a H$(C) at r(C) was set to $\approx 100\,\text{kJ mol}^{-1}$, whereas $-\Delta_a H$(D) at r(D) was set to $\approx 95\,\text{kJ mol}^{-1}$, according to the obtained experimental calorimetric and computed *ab initio* values [26]. By the inspection of the enthalpy profile illustrated in Fig. 1.25, it is clearly evident that the presence of molecularly adsorbed precursor C facilitates the rupture and formation of new chemical bonds at methoxylation site D, in that the energy barrier hindering the dissociation of methanol is dramatically lowered starting from the coordinated state instead of from the gas phase. It was calculated that coordination of CH_3OH at Ca sites is thermodynamically favored with respect to the methoxylation reaction, in agreement with the experimental results indicating that, before the prolonged contact with methanol pressure, only a fraction of the total uptake remained irreversibly bound to the surface.

1.7 Conclusions

In this preliminary Chapter it has been illustrated that adsorption microcalorimetry is very fruitfully employed in describing quantitatively the processes occurring at the gas-solid interface. The population of the surface sites active towards suitably chosen probe molecules is evaluated through the volumetric adsorption isotherms; the

surface sites heterogeneity (either structural, chemical and/or induced) is described by monitoring the evolution of the heat of adsorption with increasing coverage.

By combining the adsorption microcalorimetry results with spectroscopic and/or *ab initio* modeling methods, the knowledge of the chemical nature of the pristine surface terminations and of the adsorbed species allows to interpret at molecular level the intrinsically molar volumetric-calorimetric data. We will come back to develop this point in more details in Chap. 15.

Further, it is worth noting that much of the concepts and methods developed for characterizing the surface chemistry of solid materials of interest in heterogeneous catalysis may be used for a better understanding of the structure and properties of solid materials of interest in other fields of the material science as for instance the materials for biomedical applications (bioactive glasses, biosensors, materials for controlled drug release).

Acknowledgments Prof. Bice Fubini (University of Torino) teachings in the early stage of my work in adsorption microcalorimetry are greatly acknowledged. Further, I would like to acknowledge the contribution of Dr Claudia Busco (zeolites work, University Piemonte Orientale "A. Avogadro") and Dr Valentina Aina (Ca-modified silica work, University of Torino) in collecting the volumetric-calorimetric data published in the quoted references and employed to describe the use of adsorption microcalorimetry in surface chemistry studies. Without their enthusiasm and helpful contribution much of this work would not have been carried out. Mr Raffaele Disa (Disa Raffaele e F.lli s.a.s - Milano, I) is also greatly acknowledged for the endless, patient help in building up and maintaining the high-vacuum volumetric line.

References

1. J.M. Thomas, W.J. Thomas, *Principles and Practice of Heterogeneous Catalysis* (VCH, Weinheim (Germany), 1997)
2. R.A. Van Santen, P.W.N.M. van Leeuwen, J.A. Moulijn, B.A. Averill, *Catalysis an Integrated Approach. Studies in Surface Science and Catalysis*, vol 123 (Elsevier, Amsterdam, 1999)
3. L.L. Hench, J. Wilson, *Introduction to Bioceramics* (World Scientific, Singapore, 1993)
4. D.F. Williams, J. Black, P.J. Doherty, *Advances in Biomaterials: Biomaterial-Tissue Interfaces*, vol. 10 (Elsevier Science, Amsterdam, 1992)
5. B. Kasemo, Biological surface science. Curr. Opin. Solid State Mater. Sci. **3**(5), 451–459 (1998). doi:10.1016/S1359-0286(98)80006-5
6. B. Kasemo, Biological surface science. Surf. Sci. **500**(1–3), 656–677 (2002). doi:10.1016/S0039-6028(01)01809-X
7. R. Schlogl, in *Handbook of Heterogeneous Catalysis*, vol. 8, 2nd edn., ed. by G. Ertl, H. Knozinger, F. Schuth, J. Weitkamp (Wiley-VCH Verlag, Weinheim, 2008)
8. G. Ertl, in *Encyclopedia of Catalysis*, vol. 1, ed. by J.T. Horvath (John Wiley & Sons, Hoboken, NJ, 2003), pp. 329–352
9. A. Zecchina, D. Scarano, S. Bordiga, G. Spoto, C. Lamberti, Surface structures of oxides and halides and their relationships to catalytic properties. Adv. Catal. **46**, 265–397 (2001). doi:10.1016/S0360-0564(02)46024-5
10. Gravelle PC, in *Heat-Flow Microcalorimetry and Its Application to Heterogeneous Catalysis*, ed. by D.D. Eley HP, Paul BW. Advances in Catalysis, vol 22 (Academic Press, 1972). pp. 191–263

11. V. Bolis, G. Della Gatta, B. Fubini, E. Giamello, L. Stradella, G. Venturello, Identification of surface sites on potentially catalytic solids by adsorption calorimetry. Gazz Chim Ital **112**, 83–89 (1982)
12. B. Fubini, Adsorption Calorimetry in Surface-Chemistry. Thermochim. Acta **135**, 19–29 (1988)
13. N. Cardona-Martinez, J.A. Dumesic, Applications Of adsorption microcalorimetry to the study of heterogeneous catalysis. Adv. Catal. **38**, 149–244 (1992). doi:10.1016/s0360-0564(08)60007-3
14. A. Auroux, *Physical Techniques for Solid Materials* (Plenum Press, New York, 1994)
15. V. Bolis, A. Cavenago, B. Fubini, Surface heterogeneity on hydrophilic and hydrophobic silicas: Water and alcohols as probes for H-bonding and dispersion forces. Langmuir **13**(5), 895–902 (1997). doi:10.1021/la951006i
16. V. Bolis, S. Bordiga, C. Lamberti, A. Zecchina, A. Carati, F. Rivetti, G. Spano, G. Petrini, Heterogeneity of framework Ti(IV) in Ti-silicalite as revealed by the adsorption of NH_3. Combined calorimetric and spectroscopic study. Langmuir **15**(18), 5753–5764 (1999). doi:10.1021/la981420t
17. V.A. Basiuk in *Encyclopedia of Surface and Colloid Science*, ed. by S. Ponisseril. Adsorption of Biomolecules at Silica, (Marcel Dekker, Inc., New York, 2002), p. 277
18. V. Bolis, B. Fubini, E. Garrone, C. Morterra, Thermodynamic and vibrational characterization of CO adsorption on variously pretreated anatase. J. Chem. Soc. Faraday Trans. I **85**, 1383–1395 (1989). doi:10.1039/f19898501383
19. C. Morterra, V. Bolis, B. Fubini, L. Orio, T.B. Williams, A Ftir and Hrem study of some morphological and adsorptive properties of Monoclinic ZrO_2 microcrystals. Surf. Sci. **251**, 540–545 (1991). doi:10.1016/0039-6028(91)91051-X
20. V. Bolis, G. Magnacca, C. Morterra, Surface properties of catalytic aluminas modified by alkaline-earth metal cations: a microcalorimetric and IR-spectroscopic study. Res. Chem. Intermed. **25**(1), 25–56 (1999). doi:10.1163/156856799X00374
21. V. Bolis, S. Maggiorini, L. Meda, F. D'Acapito, G.T. Palomino, S. Bordiga, C. Lamberti, X-ray photoelectron spectroscopy and x-ray absorption near edge structure study of copper sites hosted at the internal surface of ZSM-5 zeolite: A comparison with quantitative and energetic data on the CO and NH_3 adsorption. J. Chem. Phys. **113**(20), 9248–9261 (2000). doi:10.1063/I.1319318
22. E. Garrone, V. Bolis, B. Fubini, C. Morterra, Thermodynamic and spectroscopic characterization of heterogeneity among adsorption Sites—CO on anatase at ambient-temperature. Langmuir **5**(4), 892–899 (1989). doi:10.1021/la00088a002
23. V. Bolis, A. Barbaglia, S. Bordiga, C. Lamberti, A. Zecchina, Heterogeneous nonclassical carbonyls stabilized in Cu(I)- and Ag(I)-ZSM-5 zeolites: Thermodynamic and spectroscopic features. J. Phys. Chem. B **108**(28), 9970–9983 (2004). doi:10.1021/Jp049613e
24. V. Bolis, C. Busco, S. Bordiga, P. Ugliengo, C. Lamberti, A. Zecchina, Calorimetric and IR spectroscopic study of the interaction of NH_3 with variously prepared defective silicalites—Comparison with ab initio computational data. Appl. Surf. Sci. **196**(1–4), 56–70 (2002). doi:10.1016/S0169-4332(02)00046-6
25. V. Bolis, C. Busco, P. Ugliengo, Thermodynamic study of water adsorption in high-silica zeolites. J. Phys. Chem. B **110**(30), 14849–14859 (2006). doi:10.1021/Jp061078q
26. V. Bolis, C. Busco, V. Aina, C. Morterra, P. Ugliengo, Surface properties of silica-based biomaterials: Ca species at the surface of amorphous silica as model sites. J. Phys. Chem. C **112**(43), 16879–16892 (2008). doi:10.1021/Jp805206z
27. M. Corno, A. Rimola, V. Bolis, P. Ugliengo, Hydroxyapatite as a key biomaterial: quantum-mechanical simulation of its surfaces in interaction with biomolecules. Phys. Chem. Chem. Phys. **12**(24), 6309–6329 (2010). doi:10.1039/C002146f
28. M. Armandi, V. Bolis, B. Bonelli, C.O. Arean, P. Ugliengo, E. Garrone, Silanol-Related and Unspecific Adsorption of Molecular Ammonia on Highly Dehydrated Silica. J. Phys. Chem. C **115**(47), 23344–23353 (2011). doi:10.1021/Jp206301c

29. V. Bolis, C. Busco, G. Martra, L. Bertinetti, Y. Sakhno, P. Ugliengo, F. Chiatti, M. Corno, N. Roveri, Coordination chemistry of Ca sites at the surface of nanosized hydroxyapatite: interaction with H_2O and CO. Philos. Trans. R. Soc. A: Math. Phys. Eng. Sci. **370**(1963), 1313–1336 (2012). doi:10.1098/rsta.2011.0273
30. G. Attard, C. Barnes (1998) *Surfaces. Oxford Chemistry Primers N. 59* (Oxford Science Publications, Oxford, 1998)
31. I.M. Campbell, *Catalysis at Surfaces* (Chapman and Hall, London and New York, 1988)
32. S.J. Gregg, K.S.W. Sing, *Adsorption, Surface Area and Porosity* (Academic Press, London, 1982)
33. J.A. Rabo, *Zeolites Chemistry and Catalysis*, vol. 171 (ACS Monograph American Chemical Society, Washington, D.C., 1976)
34. D.W. Breck, *Zeolites Molecular Sieves*, vol. 4 (John Wiley, New York, 1974)
35. W.M. Meier, D.H. Olson *Atlas of Zeolites Structure Types*, 2nd edn. (Butterworths, London, 1993)
36. E.M. Flanigen, J.M. Bennett, R.W. Grose, J.P. Cohen, R.L. Patton, R.M. Kirchner, J.V. Smith, Silicalite, a new hydrophobic crystalline silica molecular sieve. Nature **271**(5645), 512–516 (1978)
37. W.O. Haag, R.M. Lago, P.B. Weisz, The active site of acidic aluminosilicate catalysts. Nature **309**(5969), 589–591 (1984). doi:10.1038/309589a0
38. A. Corma, From microporous to mesoporous molecular sieve materials and their use in catalysis. Chem Rev **97**(6), 2373–2419 (1997). doi:10.1021/cr960406n
39. A. Corma, State of the art and future challenges of zeolites as catalysts. J. Catal. **216**(1–2), 298–312 (2003). doi:10.1016/s0021-9517(02)00132-x
40. E. Garrone, B. Fubini, B. Bonelli, B. Onida, C.O. Arean, Thermodynamics of CO adsorption on the zeolite Na-ZSM-5—a combined microcalorimetric and FTIR spectroscopic study. Phys. Chem. Chem. Phys. **1**(4), 513–518 (1999). doi:10.1039/a806973e
41. C. Morterra, V. Bolis, E. Fisicaro, The hydrated layer and the adsorption of CO at the surface of TiO_2 (Anatase). Colloids Surf. **41**(1–2), 177–188 (1989). doi:10.1016/0166-6622(89)80051-4
42. C. Morterra, G. Magnacca, V. Bolis, On the critical use of molar absorption coefficients for adsorbed species: the methanol/silica system. Catal. Today **70**(1–3), 43–58 (2001). doi:10.1016/S0920-5861(01)00406-0
43. S. Brunauer, L.S. Deming, W.E. Deming, E. Teller, On a theory of the van der Waals adsorption of gases. J. Am. Chem. Soc. **62**(7), 1723–1732 (1940). doi:10.1021/ja01864a025
44. S. Brunauer, P.H. Emmett, E. Teller, Adsorption of gases in multimolecular layers. J. Am. Chem. Soc. **60**(2), 309–319 (1938). doi:10.1021/ja01269a023
45. S. Brunauer, *The Adsorption of Gases and Vapours* (Oxford University Press, Oxford, 1945)
46. I. Langmuir, The adsorption of gases on plane surfaces of glass, mica and platinum. J. Am. Chem. Soc. **40**(9), 1361–1403 (1918). doi:10.1021/ja02242a004
47. R. Shannon, Revised effective ionic radii and systematic studies of interatomic distances in halides and chalcogenides. Acta Crystallogr. A **32**(5), 751–767 (1976). doi:10.1107/S0567739476001551
48. B. Fubini, V. Bolis, A. Cavenago, P. Ugliengo, Ammonia and water as probes for the surface reactivity of covalent solids—cristobalite and silicon-carbide. J. Chem. Soc., Faraday Trans. **88**(3), 277–290 (1992). doi:10.1039/ft9928800277
49. B. Fubini, V. Bolis, A. Cavenago, E. Garrone, P. Ugliengo, Structural and induced heterogeneity at the surface of some SiO_2 polymorphs from the enthalpy of adsorption of various molecules. Langmuir **9**(10), 2712–2720 (1993). doi:10.1021/la00034a034
50. P.C. Gravelle, Application of adsorption calorimetry to the study of heterogeneous catalysis reactions. Thermochim. Acta **96**(2), 365–376 (1985). doi:10.1016/0040-6031(85)80075-7
51. G. Della Gatta, Direct determination of adsorption heats. Thermochim. Acta **96**(2), 349–363 (1985). doi:10.1016/0040-6031(85)80074-5
52. A. Auroux, Acidity characterization by microcalorimetry and relationship with reactivity. Top. Catal. **4**(1–2), 71–89 (1997). doi:10.1023/A:1019127919907

53. B. Fubini, Rev. Gen. Thermique **18**, 297 (1979)
54. J.A. Dunne, M. Rao, S. Sircar, R.J. Gorte, A.L. Myers, Calorimetric heats of adsorption and adsorption isotherms.2. O_2, N_2, Ar, CO_2, CH_4, C_2H_6, and SF_6 on NaX, H-ZSM-5, and Na-ZSM-5 zeolites. Langmuir **12**(24), 5896–5904 (1996)
55. V. Bolis, G. Cerrato, G. Magnacca, C. Morterra, Surface acidity of metal oxides. Combined microcalorimetric and IR-spectroscopic studies of variously dehydrated systems. Thermochim. Acta **312**(1–2), 63–77 (1998). doi:10.1016/S0040-6031(97)00440-1
56. Fubini B, Bolis V, Bailes M, Stone FS (1989) The reactivity of oxides with water vapor. Solid State Ionics **32–33**, (Part 1 (0))258–272. doi:10.1016/0167-2738(89)90230-0
57. J.M. Newsam, M.M.J. Treacy, W.T. Koetsier, C.B.D. Gruyter, Structural characterization of zeolite beta. Proc. R. Soc. Lond. Math. Phys. Sci. **420**(1859), 375–405 (1988). doi:10.1098/rspa.1988.0131
58. M.M. Huang, A. Auroux, S. Kaliaguine, Crystallinity dependence of acid site distribution in HA, HX and HY Zeolites. Microporous Mater. **5**(1–2), 17–27 (1995). doi:10.1016/0927-6513(95)00028-8
59. A.L. Blumenfeld, J.J. Fripiat, Acid sites topology in aluminas and zeolites from high-resolution solid-state NMR. Top. Catal. **4**(1–2), 119–129 (1997). doi:10.1023/A:1019119718089
60. C. Otero Arean, G. Turnes Palomino, E. Escalona Platero, M. Penarroya Mentruit, Zeolite-supported metal carbonyls: sensitive probes for infrared spectroscopic characterization of the zeolite surface. J. Chem. Soc., Dalton Trans. **5**, 873–880 (1997). doi:10.1039/A604775K
61. M. Bregolato, V. Bolis, C. Busco, P. Ugliengo, S. Bordiga, F. Cavani, N. Ballarini, L. Maselli, S. Passeri, I. Rossetti, L. Forni, Methylation of phenol over high-silica beta zeolite: effect of zeolite acidity and crystal size on catalyst behaviour. J. Catal. **245**(2), 285–300 (2007). doi:10.1016/j.jcat.2006.10.024
62. V. Bolis, S. Bordiga, G.T. Palomino, A. Zecchina, C. Lamberti, Calorimetric and spectroscopic study of the coordinative unsaturation of copper(I) and silver(I) cations in ZSM-5 zeolite - Room temperature adsorption of NH3. Thermochim. Acta **379**(1–2), 131–145 (2001). doi:10.1016/S0040-6031(01)00612-8
63. C. Morterra, A. Chiorino, G. Ghiotti, E. Fisicaro, Spectroscopic study of anatase properties. Part 5—Surface modifications caused by K_2O addition. J. Chem. Soc., Faraday Trans. 1: Phys. Chem. Condensed Phases **78**(9), 2649–2659 (1982). doi:10.1039/F19827802649
64. C. Morterra, G. Ghiotti, E. Garrone, E. Fisicaro, Spectroscopic study of anatase properties. Part 3—Surface acidity. J. Chem. Soc., Faraday Trans. 1: Phys. Chem. Condensed Phases **76**, 2102–2113 (1980). doi:10.1039/F19807602102
65. M. Cerruti, G. Magnacca, V. Bolis, C. Morterra, Characterization of sol-gel bioglasses with the use of simple model systems: a surface-chemistry approach. J. Mater. Chem. **13**(6), 1279–1286 (2003). doi:10.1039/B300961k
66. E.P.L. Hunter, S.G. Lias, Evaluated gas phase basicities and proton affinities of molecules: an update. J. Phys. Chem. Ref. Data **27**(3), 413–656 (1998)
67. A. Auroux, Microcalorimetry methods to study the acidity and reactivity of zeolites, pillared clays and mesoporous materials. Top. Catal. **19**(3–4), 205–213 (2002). doi:10.1023/A:1015367708955
68. W.E. Farneth, R.J. Gorte, Methods for characterizing zeolite acidity. Chem. Rev. **95**(3), 615–635 (1995). doi:10.1021/cr00035a007
69. A. Zecchina, Otero Arean C (1996) Diatomic molecular probes for mid-IR studies of zeolites. Chem. Soc. Rev. 25 (3):187–197. doi:10.1039/cs9962500187.
70. A. Zecchina, C. Lamberti, S. Bordiga, Surface acidity and basicity: general concepts. Catal. Today **41**(1–3), 169–177 (1998). doi:10.1016/S0920-5861(98)00047-9
71. R.J. Gorte, What we do know about the acidity of solid acids? Catal. Lett. **62**, 1–13 (1999)
72. C. Otero Arean, E. Garrone, Trends in infrared spectroscopy of zeolites. Trends Inorg. Chem. **7**, 119–133 (2001)

73. V. Bolis, M. Broyer, A. Barbaglia, C. Busco, G.M. Foddanu, P. Ugliengo, Van der Waals interactions on acidic centres localized in zeolites nanocavities: a calorimetric and computer modeling study. J. Mol. Catal. A: Chem. **204**, 561–569 (2003). doi:10.1016/S1381-1169(03)00339-X
74. C. Busco, A. Barbaglia, M. Broyer, V. Bolis, G.M. Foddanu, P. Ugliengo, Characterisation of Lewis and Bronsted acidic sites in H-MFI and H-BEA zeolites: a thermodynamic and ab initio study. Thermochim. Acta **418**(1–2), 3–9 (2004). doi:10.1016/j.tca.2003.11.050
75. A. Poppl, T. Rudolf, D. Michel, A pulsed electron nuclear double resonance study of the Lewis acid site nitric oxide complex in zeolite H-ZSM-5. J. Am. Chem. Soc. **120**(19), 4879–4880 (1998). doi:10.1021/ja9741685
76. R.D. Shannon, K.H. Gardner, R.H. Staley, G. Bergeret, P. Gallezot, A. Auroux, The nature of the nonframework aluminum species formed during the dehydroxylation of H-Y. J. Phys. Chem. **89**(22), 4778–4788 (1985). doi:10.1021/j100268a025
77. P.A. Jacobs, H.K. Beyer, Evidence for the nature of true Lewis sites in faujasite-type zeolites. J. Phys. Chem. **83**(9), 1174–1177 (1979). doi:10.1021/j100472a013
78. C. Busco, V. Bolis, P. Ugliengo, Masked Lewis sites in proton-exchanged zeolites: a computational and microcalorimetric investigation. J. Phys. Chem. C **111**(15), 5561–5567 (2007). doi:10.1021/Jp0705471
79. H. Willner, F. Aubke, Homoleptic metal carbonyl cations of the electron-rich metals: their generation in superacid media together with their spectroscopic and structural characterization. Angewandte Chemie-Int Ed. Engl. **36**(22), 2403–2425 (1997). doi:10.1002/anie.199724021
80. A.J. Lupinetti, S.H. Strauss, G. Frenking, Nonclassical metal carbonyls. Prog. Inorg. Chem. **49**, 1–112 (2001). doi:10.1002/9780470166512.ch1
81. M. Armandi, B. Bonelli, I. Bottero, C.O. Arean, E. Garrone, Thermodynamic features of the reaction of ammonia with the acidic proton of H-ZSM-5 as studied by variable-temperature IR Spectroscopy. J. Phys. Chem. C **114**(14), 6658–6662 (2010). doi:10.1021/Jp100799k
82. E.G. Derouane, C.D. Chang, Confinement effects in the adsorption of simple bases by zeolites. Microporous Mesoporous Mater. **35–6**, 425–433 (2000)
83. L. Yang, K. Trafford, O. Kresnawahjuesa, J. Sepa, R.J. Gorte, D. White, An examination of confinement effects in high-silica zeolites. Russ. J. Phys. Chem. B **105**(10), 1935–1942 (2001). doi:10.1021/jp002964i
84. R.J. Gorte, D. White, Measuring sorption effects at zeolite acid sites: pursuing ideas from W.O. Haag. Microporous Mesoporous Mater. **35–36**, 447–455 (2000)
85. V. Bolis, B. Fubini, L. Marchese, G. Martra, D. Costa, Hydrophilic and hydrophobic sites on dehydrated crystalline and amorphous silicas. J. Chem. Soc., Faraday Trans. **87**(3), 497–505 (1991). doi:10.1039/ft9918700497
86. V. Bolis, C. Morterra, M. Volante, L. Orio, B. Fubini, Development and suppression of surface-acidity on monoclinic zirconia—a spectroscopic and calorimetric investigation. Langmuir **6**(3), 695–701 (1990). doi:10.1021/la00093a028
87. V. Bolis, B. Fubini, E. Garrone, E. Giamello, C. Morterra, in *Studies in Surface Science and Catalysis: Structure and Reactivity of Surfaces* , vol. 48, ed. by C. Morterra, A. Zecchina, G. Costa (Elsevier Sci. Publ. B.V., Amsterdam, 1989), pp. 159–166
88. V. Solinas, I. Ferino, Microcalorimetric characterisation of acid-basic catalysts. Catal. Today **41**(1–3), 179–189 (1998). doi:10.1016/S0920-5861(98)00048-0
89. V. Bolis, A. Barbaglia, M. Broyer, C. Busco, B. Civalleri, P. Ugliengo, Entrapping molecules in zeolites nanocavities: a thermodynamic and ab-initio study. Orig. Life Evol. Biosph. **34**(1–2), 69–77 (2004). doi:10.1023/B:ORIG.0000009829.11244.d1
90. S. Bordiga, I. Roggero, P. Ugliengo, A. Zecchina, V. Bolis, G. Artioli, R. Buzzoni, G. Marra, F. Rivetti, G. Spano, C. Lamberti, Characterisation of defective silicalites. J. Chem. Soc., Dalton Trans. **21**, 3921–3929 (2000). doi:10.1039/B004794p
91. E. Garrone, F. Rouquerol, B. Fubini, G. Della Gatta, Entropy of adsorption and related thermodynamic functions in an open isothermal system. J Chim Phys **76**, 528–532 (1979)

92. C. Otero Arean, O.V. Manoilova, G.T. Palomino, M.R. Delgado, A.A. Tsyganenko, B. Bonelli, E. Garrone, Variable-temperature infrared spectroscopy: an access to adsorption thermodynamics of weakly interacting systems. Phys. Chem. Chem. Phys. **4**(23), 5713–5715 (2002). doi:10.1039/B209299a
93. S. Savitz, A.L. Myers, R.J. Gorte, Calorimetric investigation of CO and N_2 for characterization of acidity in zeolite H-MFI. J. Phys. Chem. B **103**(18), 3687–3690 (1999). doi:10.1021/jp990157h
94. D. McQuarrie, *Statistical Mechanics* (Harper and Row, New York, 1986)
95. D.H. Everett, Thermodynamics of adsorption. Part I—General considerations. Trans. Faraday Soc. **46**, 453–459 (1950)
96. T.L. Hill, Statistical mechanics of adsorption. V. Thermodynamics and heat of adsorption. J. Chem. Phys. **17**(6), 520–535 (1949). doi:10.1063/1.1747314
97. E. Garrone, G. Ghiotti, E. Giamello, B. Fubini, Entropy of adsorption by microcalorimetry. Part 1—Quasi-ideal chemisorption of CO onto various oxidic systems. J. Chem. Soc., Faraday Trans. 1: Phys. Chem. Condensed Phases **77**(11), 2613–2620 (1981)
98. G. Busca, H. Saussey, O. Saur, J.C. Lavalley, V. Lorenzelli, Ft-Ir Characterization of the surface-acidity of different titanium-dioxide anatase preparations. Appl. Catal. **14**(1–3), 245–260 (1985). doi:10.1016/S0166-9834(00)84358-4
99. F. Rouquerol, J. Rouquerol, C. Letoquart, Use of isothermal microcalorimetry data for the determination of integral molar entropies of adsorption at the gas–solid interface by a quasi-equilibrium procedure. Thermochim. Acta **39**(2), 151–158 (1980). doi:10.1016/0040-6031(80)80008-6
100. H. Knozinger, *The Hydrogen Bond* (North Holland, Amsterdam, 1976)
101. U. Diebold, The surface science of titanium dioxide. Surf. Sci. Rep. **48**(5–8), 53–229 (2003)
102. V. Bolis, B. Fubini, E. Giamello, Effect of form on the surface-chemistry of finely divided solids. Mater. Chem. Phys. **29**(1–4), 153–164 (1991). doi:10.1016/0254-0584(91)90012-J
103. L. Kieu, P. Boyd, H. Idriss, Trends within the adsorption energy of alcohols over rutile TiO_2(110) and (011) clusters. J. Mol. Catal. A: Chem. **188**(1–2), 153–161 (2002). doi:10.1016/S1381-1169(02)00210-8
104. A.C. Zettlemoyer, F.T. Micale, K. Klier, *Water in dispersed Systems*, vol. 5 (Plenum, New York, 1975)
105. S. Savitz, A.L. Myers, R.J. Gorte, A calorimetric investigation of CO, N_2, and O_2 in alkali-exchanged MFI. Microporous Mesoporous Mater. **37**(1–2), 33–40 (2000). doi:10.1016/S1387-1811(99)00190-0
106. J.E. Jones, On the determination of molecular fields. II. From the equation of state of a gas. Proc. R. Soc. Lond. Ser. A **106**(738), 463–477 (1924). doi:10.1098/rspa.1924.0082
107. P.M. Morse, Diatomic molecules according to the wave mechanics. II. Vibrational levels. Physical Review **34**(1), 57–64 (1929). doi:10.1098/rspa.1924.0082

http://www.springer.com/978-3-642-11953-8

Calorimetry and Thermal Methods in Catalysis
Auroux, A. (Ed.)
2013, XVI, 561 p. 312 illus., 85 illus. in color., Hardcover
ISBN: 978-3-642-11953-8